

LECTURE 1

The Stochastic Gravity-Wave Background: Sources and Detection

B. Allen

*Department of Physics
University of Wisconsin - Milwaukee
PO Box 413
Milwaukee, WI 53211, USA
email: ballen@dirac.phys.uwm.edu*

1. INTRODUCTION

The design and construction of a number of new and more sensitive detectors of gravitational radiation is currently underway. These include the LIGO detector being built in the United States by a joint Caltech/MIT collaboration [1], the VIRGO detector being built near Pisa by an Italian/French collaboration [2], the GEO-600 detector being built in Hannover by an Anglo/German collaboration [3], and the TAMA-300 detector being built near Tokyo [4]. There are also several resonant bar detectors currently in operation, and several more refined bar and interferometric detectors presently in the planning and proposal stages.

It's not clear when the first sources will be detected – this may happen soon after the detectors go “on-line” or it may require decades of further work to increase the sensitivity of the instruments. But it's clear to me that eventually, when the sensitivity passes above some threshold value, the gravity-wave detectors will find sources.

The operation of these detectors will have a major impact on the field of gravitational physics. For the first time, there will be a significant amount of experimental data to be analyzed, and the “ivory tower” relativists will be forced to interact with a broad range of experimenters and data analysts to

extract the interesting physics from the data stream. Being an optimist, I think that this “interesting physics” will include sources of gravitational radiation which we have not hitherto expected or even conceived of. It promises to be an exciting time.

There are at least three major types of “known” sources [5, 6]. These are (1) coalescing binary systems, composed of neutron stars and/or black holes, (2) pulsars (and other periodic sources), and (3) supernovae (and other transient or burst sources). These are listed, roughly speaking, in increasing order of “detection difficulty”. For example, the waveforms (chirps) of the coalescing binary systems are already known to a high enough degree of precision [7, 8, 9] to enable reliable detection, using the classical signal analysis technique of matched filtering [10, 11]. Some order-of-magnitude studies have shown that the amount of required processing can be done with a dozen or so high-performance desktop workstations [12]. The major unknown for this type of source is their number density, which is uncertain by more than an order of magnitude. Hence the rate of events which occur close enough to us to be observable can not be estimated very precisely. The second type of source is pulsars. Once again, the form of the signal is known very precisely: it’s just a sine wave in the solar system barycenter, a coordinate system at rest with respect to the Sun [13]. In this case however, the signal processing problem is far more difficult, because the orbital motion of the earth around the sun and the rotational motion of the earth around its axis modulates the pulsar frequency. This means one must separately analyze the signal for each of $\approx 10^{14}$ separate patches on the celestial sphere, each of which would have a distinctive pattern of frequency modulation. The required processing speeds are currently beyond the limits of even the most powerful computers. Of course, it may be just a question of waiting until a better search algorithm is developed, or faster computers become available! The third source which I’ve listed, supernovae, is perhaps the most difficult to detect. There are two reasons. First, we do not have precise predictions of the gravitational waveform such an event would produce – and it’s hard to design a data analysis algorithm to look for something unknown. Furthermore, these explosions are expected to be rare events and because certain kinds of instrument noise might look quite similar to supernovae, I chose to list them last, and categorize them as the most difficult sources to detect.

The subject of these lectures is a fourth type of source, quite different in character from the three listed above. These are the “stochastic” or “background” sources [14, 15, 16]. Roughly speaking, these are “random” sources, typically arising from an extremely large number of “unresolved” independent and uncorrelated events. This type of background could be the result of processes that take place very shortly after the big bang, but since we know very little about the state of the universe at that time, it’s impossible to say with any certainty. Such a background might also arise from processes that take place fairly recently (say within the past several billion years) and this more recent contribution might overwhelm the parts of the background which contain information about the state of the early universe.

These sources are “unresolved” in the following sense. If we study an optical source, somewhere in the sky, using a telescope with a certain angular resolution, then details of the source can be “resolved” if the angular resolution of the telescope is smaller than the angular size of the features or objects being studied. In the case of the LIGO experiment, and similar detectors, the angular size of the antenna pattern is of order 90° . Hence almost any source is “unresolved” in that it makes a significant contribution to the detector output for almost any orientation of the detector and the source. When many such sources are present, even if they are pointlike, the resulting signal has a stochastic nature.

My motivation for studying these stochastic sources is two-fold. The first reason is a rather hopeful one. Because the gravitational force is the weakest of the four known forces, the small-scale perturbations of the gravitational field decouple from the evolution of the rest of the universe at very early times. Currently, our most detailed view of the early universe comes from the microwave background radiation, which decoupled from matter about 10^5 years after the big bang, and gives us an accurate picture of the universe at this rather early time. Some rather simple estimates (which I’ll elaborate later) show that if the current crop of gravity-wave detectors do detect a background of cosmological origin, then it will carry with it a picture of the universe as it was about 10^{-22} seconds after the big bang. This would represent a tremendous step forward in our knowledge, and is the main reason for my interest.

The second reason for my interest in stochastic sources is rather more practical. One often hears it said that searching for signals in the output of a gravitational wave antenna is like searching for a needle in a haystack. And indeed, for the first three types of source listed above, this is true. One has to search through tons of rock (the data stream) in order to find the one precious gem (say, a binary chirp). Most of the rock is barren, and the challenge is to isolate the one tiny volume containing the material of interest. As I have already discussed, for gravitational wave sources, the amount of computational power required for this careful search can be very large. However the situation is rather different when one is searching for a stochastic background. The analogy in this case is mining aluminum, where on average every ton of ore contains a certain number of kilograms of aluminum. The situation is analogous for stochastic gravity-wave sources. As you will see, whenever two detectors are operating simultaneously, even if only for a few seconds, we get a little bit more data and information about the stochastic background. And as you will also see, it is easy to analyze this data. The “signal” in this case is a very low bandwidth one, so the essential part of the data analysis for a stochastic background can be done on a garden-variety personal computer. For example, in the case of the LIGO detectors, the part of the signal carrying a significant amount of information lies below a few hundred Hz (see Section 3.3 and Fig. 7 for details). Thus the rate at which information needs to be processed is only a few hundred data points/second; a very manageable rate.

These lectures are organized as follows. In Section 2, I discuss some of the general properties that a stochastic background of gravitational radiation might

have. I show how such radiation is characterized by a spectral function, discuss some of its statistical properties, and show during which cosmological epoch the radiation which falls into the bandwidth of the ground- and space-based detectors was produced. In Section 3 I show how one can combine data from two or more gravity-wave detectors to either put limits on the amplitude of a stochastic background, or to actually detect it. I do this in several steps, first giving a crude argument which demonstrates the main detection strategy, then discussing the reduction in sensitivity which comes about from the siting of the detectors and their relative orientations on the earth. This is followed by a rigorous derivation of the optimal signal processing strategy, and a calculation of the expected signal-to-noise ratio and the minimum detectable energy-density in a stochastic background. In Section 4 I discuss the observational facts: what we actually know about the stochastic background. There are strong limits on the spectrum of a stochastic background coming at very long wavelengths from observations of the isotropy of the Cosmic Microwave Background Radiation, and limits at higher frequencies from observations of timing residuals in millisecond pulsars. Finally, there is a limit on the integrated spectrum arising from the standard model of big bang nucleosynthesis. The last part of these lectures is far more speculative. In Section 5 I discuss some of the potential ways in which a stochastic background might arise from processes that take place early in the history of the universe. I discuss in some detail three particular models (inflation, cosmic strings, and bubble formation in a first-order phase transition) each of which gives rise to a different spectrum of radiation, and examine in some detail the mechanisms at work in each case. In each case I indicate if and when the experiments being built might detect these potential sources. This is followed by a short conclusion, and an appendix containing a few calculational details.

2. THE STOCHASTIC BACKGROUND: SPECTRUM & PROPERTIES

2.1. Digression - the Cosmic Microwave Background Radiation

In order to discuss the spectrum of gravitational background radiation, we need to introduce notation. I will do this with an analogy and an example.

Let's begin by considering the electromagnetic background radiation, conventionally referred to as the Cosmic Microwave Background Radiation (CMBR) [17]. This radiation was originally produced when the universe had a temperature of about 3000 K, at a redshift of approximately $Z = 1100$. Today, this electromagnetic radiation has a Planck blackbody spectrum with a temperature of about $T = 2.73$ K. Each cubic centimeter around us contains ≈ 400 CMBR photons of energy $\approx 10^{-15}$ erg. The total energy density in this radiation field is $\rho_{\text{em}} = 4.2 \times 10^{-13}$ ergs/cm³, and the characteristic frequency of the photons that make it up is (a few times) $f_0 = kT/h = 5.7 \times 10^{10}$ Hz. Here

$h = 6.6 \times 10^{-27}$ erg – sec is Planck's constant, $k = 1.4 \times 10^{-16}$ erg/Kelvin is Boltzmann's constant.

In order to characterize the spectral properties of this radiation, we'll now consider how this energy is distributed in frequency. In a spatial volume V , the amount of energy dE contained in this radiation field between frequencies f and $f + df$ can be expressed as

$$dE = (2)hf \left(\frac{1}{e^{hf/kT} - 1} \right) \left(\frac{4\pi V f^2 df}{c^3} \right), \quad (1)$$

where $c = 3 \times 10^{10}$ cm/sec is the speed of light. The different factors appearing on the right hand side of this equation are (1) the number of polarizations (2) the energy per quanta (3) the number of quanta per mode, and (4) the number of modes in the frequency interval. Dividing both sides of this equation by the volume V , one may write the energy density within the frequency range df as

$$d\rho_{\text{em}} \equiv \frac{dE}{V} = \frac{8\pi h}{c^3} \frac{f^3 df}{e^{hf/kT} - 1}. \quad (2)$$

It will prove convenient to write the differential energy density within a unit *logarithmic* frequency interval. This is

$$\frac{d\rho_{\text{em}}}{d \ln f} = f \frac{d\rho_{\text{em}}}{df} \approx 3.8 \times 10^{-14} \frac{\text{ergs}}{\text{cm}^3} \left(\frac{f}{f_0} \right)^4 \left(\frac{e - 1}{e^{f/f_0} - 1} \right). \quad (3)$$

This formula contains complete information about the spectral distribution of energy in the CMBR, and if we were interested in discussing electromagnetic backgrounds, we would probably stop here. However there is a slightly different standard convention used to describe gravitational wave backgrounds.

In describing gravitational wave stochastic backgrounds, it is conventional to *compare* the energy density to the critical energy density ρ_{critical} required (today) to close the universe. This critical energy density is determined by the rate at which the universe is expanding today. Let us denote the Hubble expansion rate today by

$$H_0 = h_{100} 100 \frac{\text{Km}}{\text{sec} - \text{Mpc}} = 3.2 \times 10^{-18} h_{100} \frac{1}{\text{sec}} = 1.1 \times 10^{-28} h_{100} \frac{1}{\text{cm}}. \quad (4)$$

Because we don't know an accurate value for H_0 (a matter of considerable controversy in the literature) we include a dimensionless factor of h_{100} which almost certainly lies within the range $1/2 < h_{100} < 1$. The critical energy-density required to just close the universe is then given by

$$\rho_{\text{critical}} = \frac{3c^2 H_0^2}{8\pi G} \approx 1.6 \times 10^{-8} h_{100}^2 \frac{\text{ergs}}{\text{cm}^3}. \quad (5)$$

This leads to our fundamental definition in this section, of a quantity which we will be using for the remainder of these lectures.

In the remainder of these lectures, we will be discussing gravitational wave, rather than electromagnetic backgrounds. However, to complete this section, we first define the analogous quantity for electromagnetic backgrounds. This quantity is a dimensionless function of frequency

$$\Omega_{\text{em}}(f) \equiv \frac{1}{\rho_{\text{critical}}} \frac{d\rho_{\text{em}}}{d \ln f}. \quad (6)$$

For the thermal spectrum of electromagnetic radiation in the CMBR, we have

$$\Omega_{\text{em}}(f) = 2.4 \times 10^{-6} h_{100}^{-2} \left(\frac{f}{f_0} \right)^4 \left(\frac{e-1}{e^{f/f_0} - 1} \right). \quad (7)$$

A graph this function is shown in Fig. 1. Also shown in Fig. 1 is the spectrum that the gravitational wave stochastic background would have, if at early times in the history of the universe the fluctuations in the gravitational field had been in equilibrium with the other matter and radiation in the universe. In this case, the gravitational wave stochastic background would have a thermal spectrum, with a temperature of about 0.9 K [17]. It is smaller than the temperature of the CMBR because in a conventional hot big bang model, the gravitons would have decoupled when the temperature of the universe dropped below the Planck temperature, when the number of entropy degrees of freedom was 106.75 in the standard GUT model. Since the number of degrees of freedom today is only 3.91, the graviton temperature is less than that of the CMBR by the ratio $(106.75/3.91)^{1/3}$. (See discussion in [17], pg 75, between (3.89) and (3.90)). However it is unlikely that this equilibrium could have been established; the time required to establish the equilibrium is longer than the characteristic expansion time (the Hubble time) of the universe because the gravitational interaction is so weak. While it is therefore unlikely that this 0.9 K thermal spectrum is present, it is nevertheless a useful benchmark for comparison.

A number of graphs similar to Fig. 1 will appear in these lectures, so a couple of comments are in order. First, the reader will notice that the horizontal axis encompasses an *enormous* range of frequencies. The lowest frequencies $f \approx H_0$ are those of waves which only oscillate a single time in the entire history of the universe, and whose period is a Hubble time H_0^{-1} ! The highest frequencies shown are those of visible light. Second, these graphs make it easy to see the total amount of energy contributed by the radiation to the energy density of the universe. From the vertical axis, one can immediately see from the graph of $\Omega_{\text{em}}(f)$ that the CMBR contains, in the vicinity of 10^{11} Hz, about 10^{-5} of the energy required to close the universe.

2.2. Notation - the Spectral Function $\Omega(f)$ for Gravitational Waves

In order to characterize the spectrum of a stochastic gravitational wave signal, we introduce a quantity for the graviton background which is analogous to Ω_{em} .

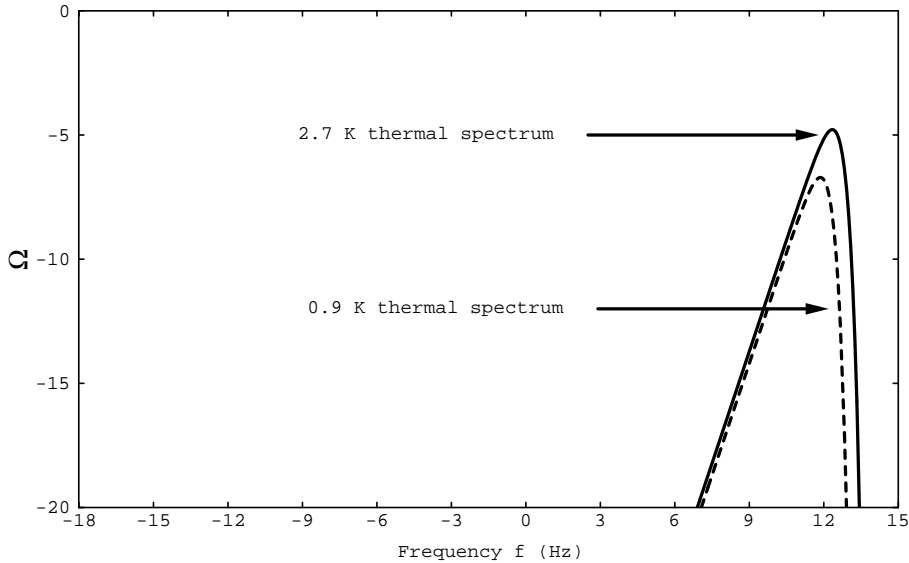


Fig. 1. — The solid curve is the fractional energy density $\Omega_{\text{em}}(f)$ contained in the 2.73 K electromagnetic background radiation (with h_{100} set to unity). The dashed curve shows the corresponding quantity for a 0.9 K blackbody. If the gravitational perturbations had been in equilibrium with the matter fields, this is the expected spectrum of the gravitational wave stochastic background. Both axes are \log_{10} .

The precise definition is

$$\Omega(f) = \Omega_{\text{gw}}(f) \equiv \frac{1}{\rho_{\text{critical}}} \frac{d\rho_{\text{gw}}}{d \ln f}. \quad (8)$$

The subscripts “gw” for “gravitational wave” are omitted when there is no danger of ambiguity.

There appears to be some confusion about $\Omega(f)$ in the literature. Some authors assume that $\Omega(f)$ is independent of frequency f ; this is true for some cosmological models, but not for all of them. The important thing is that *any* spectrum of gravitational radiation can be described by an appropriate $\Omega(f)$. With the correct dependence on frequency f it can describe a flat spectrum, or a black-body spectrum, or any other specific distribution of energy with frequency.

You will also notice that it follows directly from the definition that the quantity $h_{100}^2 \Omega(f)$ is independent of the actual Hubble expansion rate. For this reason, we will often focus attention on that quantity, rather than on $\Omega(f)$ alone.

It is sometimes convenient to discuss the spectrum of gravitational waves and the sensitivity of detectors in terms of a characteristic “chirp” amplitude.

This is the dimensionless gravitational-wave strain $h = \Delta L/L$ that would be produced in the arms of a detector, in a bandwidth equal to the observation frequency. This is related to $\Omega(f)$ by

$$h_c(f) = 1.3 \times 10^{-20} h_{100} \sqrt{\Omega(f)} \frac{100 \text{ Hz}}{f}. \quad (9)$$

(Equation 65 of [18]). Apart from an overall factor, this formula can be easily derived by dropping the time derivatives from (A13). For example if $\Omega(f) = 10^{-8}$ over a bandwidth $50 \text{ Hz} < f < 150 \text{ Hz}$ then the strain in an ideal detector is $h_c \approx 10^{-24}$.

2.3. Assumptions about the Stochastic Gravitational-Wave Background

Does $\Omega(f)$ contain all information about the stochastic background? The answer is “yes” provided that we make enough additional assumptions.

We will assume from here on that the stochastic gravity wave background is isotropic, stationary, and Gaussian; under these conditions it is completely specified by its spectrum $\Omega(f)$. Each of these three properties might or might not hold; before moving on, let’s consider each in turn.

It is now well established that the CMBR is highly isotropic [17]. In fact this isotropy is surprising, because in the standard model of cosmology, the angular size of the horizon at $Z = 1100$ is only about 2° . Nevertheless, it is experimentally well-established that the largest deviation from the isotropy of the CMBR arises from our proper motion with respect to the rest frame of the universe, at the level of 1 part in 10^3 . The next largest deviations from isotropy arise at the level of 1 part in 10^5 ; these fluctuations arise because of the non-uniform distribution of matter at (and after) the surface of last scattering.

It is therefore not unreasonable to assume that the stochastic gravity wave background is also isotropic. However this assumption may not be true. For example, suppose that the dominant source of stochastic gravity wave background is a large number of unresolved white dwarf binaries within our own galaxy. Because our galaxy is bar or spiral shaped (and not spherical) if we assume that the white dwarf binaries are distributed in space in the same way as the matter in the galaxy, then the stochastic background will have a distinctly anisotropic distribution, and will form a “band in the sky” distributed roughly in the same way as the milky way. It is also possible for a stochastic gravity wave background of cosmological origin to be quite anisotropic. Of course in this case, one is left with the problem of explaining why the CMBR is isotropic, but the gravity wave background is not. It is possible to conceive of such mechanisms, but within the scope of these lectures, we will not consider their effects.

The assumption that the stochastic background is stationary is almost certainly justified. Technically this means that the n -point correlation functions of the gravitational wave fields depend only upon the differences between the

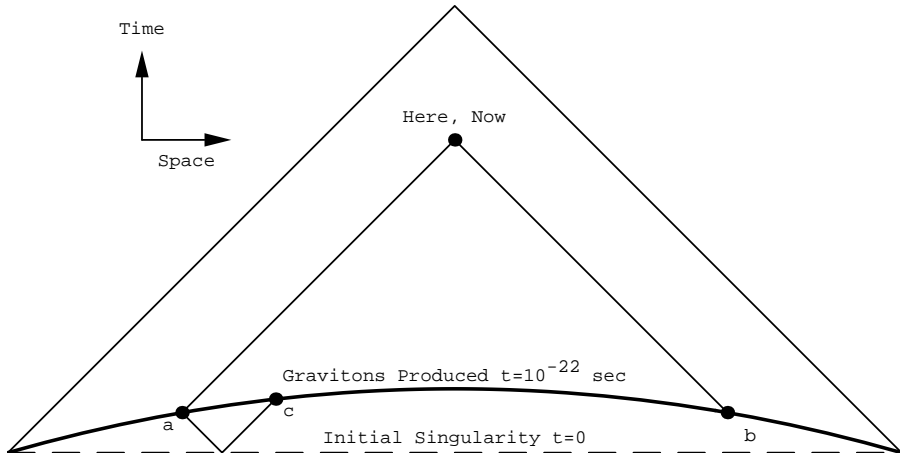


Fig. 2. — A conformal diagram showing a spatially-flat Friedman-Robertson-Walker cosmological model. The past light cone of a present-day observer (Here, Now) intersects a surface at $t = 10^{-22}$ seconds in a large 2-sphere, of which two points (a,b) are shown. The future light cone of the initial singularity intersects the same surface in a much smaller 2-sphere, of which two points (a,c) are also shown. The number of independent, uncorrelated horizon volumes N_{horizon} which contribute to the gravitational radiation arriving at a detector today is given by the ratio of the areas of the larger 2-sphere to the smaller one.

times, and not on the choice of the time origin. Because the age of the universe is 20 orders of magnitude larger than the characteristic period of the waves that LIGO, VIRGO, and the other facilities can detect, and 9 orders of magnitude larger than the longest realistic observation times, it seems very unlikely that the stochastic background has statistical properties that vary over either of these time-scales.

The final assumption we make is that the fields are Gaussian, by which we mean that the joint density function is a multivariate normal distribution. For many early-universe processes which give rise to a stochastic background, this is a reasonable assumption, which can be justified with the central limit theorem. Let's sketch the argument out.

We will show in Section 2.4 that if the stochastic background arises from processes that take place in the early universe, the characteristic time (proper time after the big bang) at which the gravitational radiation was emitted was about $t = 10^{-22}$ sec. Consider the conformal diagram [19], shown in Fig. 2. As Fig. 2 graphically illustrates, a detector today located at the spacetime point labeled "Here, Now" observes radiation produced at $t = 10^{-22}$ seconds after the big bang by an extremely large number N_{horizon} of independent horizon volumes. We can estimate the number of these horizon-sized volumes on the

surface $t = 10^{-22}$ seconds as follows.

Let's assume that the universe is $k = 0$ (spatially flat) and radiation dominated from the time that the gravitons were produced ($t_1 = 10^{-22}$ sec) until the present time ($t_0 = 10^{17}$ sec). This is a reasonable assumption for this type of calculation; although the universe did recently become matter dominated (at a redshift of a few thousand) this has only a small effect on the final answer. The redshift Z of the $t = t_1$ constant-time surface is then given by $1 + Z = (10^{17}/10^{-22})^{1/2} \approx 10^{20}$. Let's work in a "conformal time" coordinates where $ds^2 = a^2(\eta)(-d\eta^2 + d\vec{x}^2)$. For a radiation-dominated universe $a(\eta) = \eta$, and we can take the present time to have $\eta = \eta_0$ and the time at which gravitons were produced to have $\eta = \eta_1$. We begin by considering the intersection of the forward light cone of the initial singularity with the surface $\eta = \eta_1$. This intersection forms the small two-sphere denoted by the points "a" and "c" in Fig. 2; this two-sphere has area $A_{\text{small}} = 4\pi\eta_1^2 a^2(\eta_1)$. In similar fashion, the past light cone of the present-day detector intersects the surface $\eta = \eta_1$ in the large two sphere denoted by the points "a" and "b", which has area $A_{\text{big}} = 4\pi(\eta_0 - \eta_1)^2 a^2(\eta_1)$. The ratio of these two areas is the number of horizon volumes visible to the detector over the entire sky; it is

$$N_{\text{horizon}} = \frac{A_{\text{big}}}{A_{\text{small}}} = \frac{(\eta_0 - \eta_1)^2}{\eta_1^2} = Z^2 \approx 10^{39}. \quad (10)$$

If we assume that the processes producing gravitational waves from each of these separate horizon volumes act independently, then it follows immediately from the central limit theorem that the amplitude of the radiation arriving at the detector, which is the sum of the amplitudes of the radiation produced by each of the separate volumes, is Gaussian.

2.4. When is a Stochastic Background produced?

Suppose that the LIGO or VIRGO detectors do detect a stochastic background of gravitational radiation. From what epoch, in the history of the universe, does this radiation date?

To give a general answer to this question, we need to make some assumptions about the universe. The most reasonable thing to do is to adopt the "standard model" of cosmology. This cosmological model consists of a spatially-flat ($k = 0$ Friedman-Robertson-Walker) cosmological model, in which the equation of state is dominated by massless (or highly relativistic) matter for redshifts greater than $Z_{\text{eq}} \approx 6000$, and is dominated by massive pressureless particles (dust!) for smaller redshifts.

The question posed above has two answers, one mundane, the other quite exciting. The mundane possibility is that the radiation was produced at or near the present epoch (say, within a redshift $Z < 4$) by many unresolved separate sources, such as white dwarf binaries or supernovae. For example, in the case of the electromagnetic background radiation, one finds that below about 300 MHz the spectrum is dominated by (recent) emission from our own galaxy [20]. The

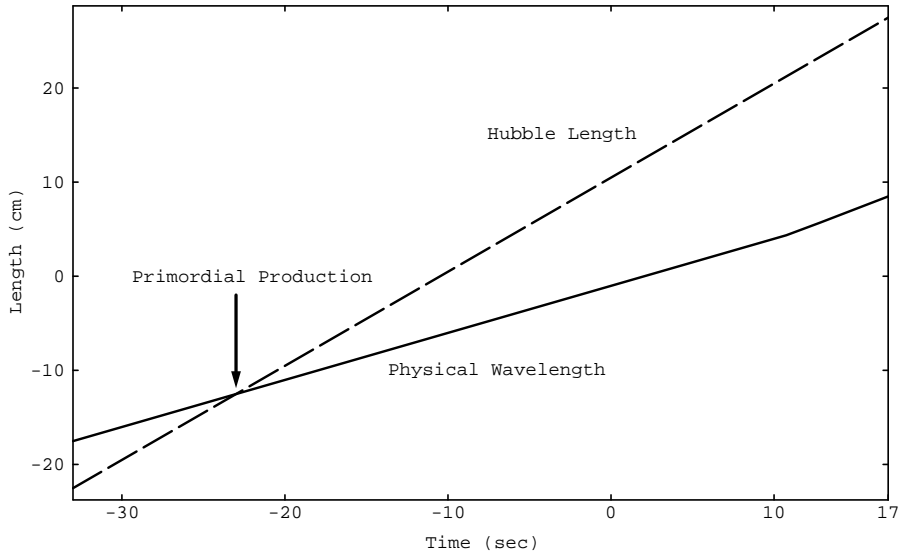


Fig. 3. — This graph shows the two lengths, as functions of cosmological time (both axes are \log_{10}). Today, we are at the far right of the graph, $t \approx 10^{17}$ seconds after the big bang. The solid curve shows the physical wavelength of a wave that LIGO or VIRGO might detect, at ≈ 100 Hz. Today this wavelength is about 3×10^8 cm; in the past this wavelength shrinks because of redshifting, in proportion to the cosmological scale factor, first as $t^{2/3}$ when the universe is matter dominated, then as $t^{1/2}$ when the universe is radiation dominated. The dotted curve shows the characteristic spatial size (and age) of the universe, the Hubble length, which today is $\approx 10^{28}$ cm. This function grows $\propto t$. The intersection of these two curves determines the time at which the primordial production of gravitons in the LIGO/VIRGO band took place.

more exciting possibility is that such gravitational radiation is a cosmological fossil. In the case of the electromagnetic spectrum, at frequencies above 1 GHz, this is indeed the case.

Let us assume that the LIGO or VIRGO detectors do detect a stochastic background of gravitational radiation, and let us also assume that this radiation has a cosmological (a long time ago) rather than a local (recently) origin. The time at which this radiation was produced can be determined by simple physical argument. The production of gravitational radiation is no different than the production of any other type of radiation. If we want to produce electromagnetic radiation at 1 KHz, we need to take electric charges and vibrate them at 1 KHz. The same holds for gravitational radiation; waves of a certain frequency are produced when the characteristic time for the matter and energy in the universe to shift about is comparable to the period of the waves. The graph in Fig. 3 shows two length scales, as functions of cosmic time. As

can be seen from the diagram, at about 10^{-22} seconds after the big bang the characteristic expansion time (the Hubble time) was about comparable to the period of a wave, which when redshifted to the present epoch, falls within the bandwidth of LIGO/VIRGO sensitivity.

The most exciting prospect in the study of the stochastic background is the possibility of detecting radiation produced at this very early epoch of $t \approx 10^{-22}$ sec. To give a sense for the scales, a 100 Hz graviton detected by the LIGO experiment was produced at that early epoch with an energy of order 10 MeV. The mean temperature in the universe at that time was of order 10^7 GeV. For this reason, detecting a background of cosmological origin would give us a glimpse of the universe at *much* earlier times than we can obtain in other ways.

Comparable calculations can be done for the proposed Laser Interferometer Space Antenna (LISA) experiment [21], which is designed to detect waves with frequencies in the range $\approx 10^{-4}$ Hz to $\approx 10^{-1}$ Hz. In this case, one finds that waves of cosmological origin with present-day frequency $\approx 10^{-2}$ Hz were produced at time of order 10^{-14} sec after the big bang; at the time of their production the energy of the gravitons was ≈ 0.1 eV. The overall temperature of the universe at this time was $\approx 10^3$ GeV - a particularly interesting epoch, because the electro-weak phase transition occurred around that energy scale.

3. Experimental Detection Methods and their Sensitivity

3.1. How to Detect a Stochastic Background (Crude Version)

In these lectures, I'd like to answer the question "how does one actually use the output from the gravitational wave detectors to find (or place upper limits on) a stochastic gravity wave background." Later, in Section 3.3 we will re-visit this question and give a very precise (in fact, optimal) answer to this question. However my goal here is to give a rough understanding of the method and its limitations.

Now in general, there are two possibilities. First, when a detector is operating, its intrinsic noise level might be lower than the random stochastic signal arising from the gravitational wave background. In this case, no clever signal detection strategies are required. One simply "turns on" the detector, studies its output for a few seconds, and concludes that a stochastic background is present. In a crude sense, this is how Penzias and Wilson discovered the electromagnetic CMBR; the signal it produced was greater than the intrinsic noise of their detector. Of course it was not quite so easy - Penzias and Wilson had to spend an entire summer studying the intrinsic noise in their radio telescope before they could be sure that the excess noise they were observing was of cosmological origin!

Let us assume that the signal levels produced by the stochastic background of gravitational radiation are not this large, so that the output of a detector is dominated by the noise produced within the detector rather than by the signal

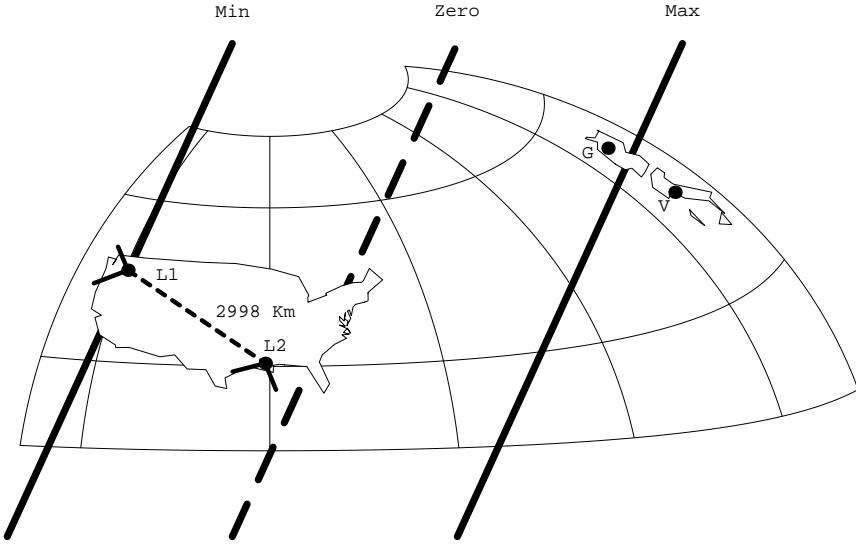


Fig. 4. — Shown is the surface of the earth $15^\circ < \text{latitude} < 75^\circ$, and $-130^\circ < \text{longitude} < 20^\circ$, including the LIGO detectors in Hanford, WA (L1) and Livingston, LA (L2) and the locations of the VIRGO detector (V) in Pisa, Italy and the GEO-600 (G) detector in Hannover, Germany. The perpendicular arms of the LIGO detectors are also illustrated (though not to scale). A plane gravitational wave passing by the earth is indicated by successive minima (troughs), zeros, and maxima (peaks) of the wave. As this wave passes by the pair of LIGO detectors, it excites the detectors in coincidence at the moment shown, because both detectors are driven negative by the wave. During the time when the zero is between L1 and L2, the two detectors respond in anti-coincidence. Provided that the wavelength λ of the wave is larger than about twice the separation distance (2998 Km) between the detectors, on the average they are driven in coincidence more of the time than in anti-coincidence.

due to the stochastic background itself. In this case, as was first shown by Michelson [14] one can still detect the signal due to a stochastic background, by correlating the outputs of two different detectors. The principal requirement that must be met by the two detectors is that they must have *independent noise*. Later in these lectures we will be more specific about what is required.

In the case where we have two detectors, one can isolate the signal due to the stochastic background by correlating their outputs. As can be seen from Fig. 4, a gravitational plane wave passing by the earth excites a pair of detectors in coincidence when the positive or negative amplitude part of the wave is passing by both detectors at the same time (in the rest frame of the detectors). It excites the detectors in anti-coincidence during moments when the positive amplitude part of the wave is passing by one detector, and

the negative amplitude part of the wave is passing by the other detector, or vice versa. Provided that the wavelength of the wave is much larger than twice the distance between the two detectors, on the average the detectors will be driven in coincidence. In the case of the LIGO detector pair, below a frequency of 64 Hz, the Hanford and Livingston detectors will be driven (on the average) in coincidence by an unpolarized isotropic stochastic background. This can be seen by inspecting Fig. 5; the first zero of this function lies at $f = 64$ Hz. We note that this result is slightly higher than the frequency (50 Hz) associated with a wavelength of twice the detector separation (6000 Km) because the overlap reduction function is a sum of Bessel functions (21) which does not vanish at 50 Hz.

The basic idea (the optimal implementation is elaborated in Section 3.3) is to multiply together the outputs of the two independent detectors, and integrate the result. For the purpose of this section, imagine that two detectors are located at the same point, and have identical orientations. In our case, for frequencies well below 64 Hz, the LIGO detectors may be thought of as “being at the same point”. In similar fashion, although the LIGO detectors are not identically oriented (they are 22.7° apart as seen from the center of the earth, and thus can not lie in the same plane) their arms are as close to parallel as is possible given their separation.

In this simplified case the output of the first detector is

$$s_1(t) = h_1(t) + n_1(t), \quad (11)$$

where h_1 is the strain due to the stochastic background and n_1 is the intrinsic noise of the first detector. In similar fashion, the output of the second detector is

$$s_2(t) = h_2(t) + n_2(t). \quad (12)$$

Since we are assuming that the two detectors have identical locations and orientations then the gravity-wave strains are identical: $h_1(t) = h_2(t)$. We can form a “signal” by multiplying together the outputs of the two detectors and integrating:

$$S = \langle s_1, s_2 \rangle \equiv \int_{-T/2}^{T/2} s_1(t)s_2(t)dt. \quad (13)$$

Here T is the integration time (realistically, a few months). There are two different cases to consider. As we explained earlier, the case where the detector noise n_i is small compared to the signal s_i not very interesting, as one can find the background easily in that case. So we’ll assume that the signal is small compared to the detector noise, in which case we can write

$$S = \langle h_1, h_2 \rangle + \langle n_1, h_2 \rangle + \langle h_1, n_2 \rangle + \langle n_1, n_2 \rangle \quad (14)$$

$$\approx \langle h_1, h_2 \rangle + \langle n_1, n_2 \rangle. \quad (15)$$

where we have dropped terms like $\langle n_1, h_2 \rangle$ that are smaller than $\langle n_1, n_2 \rangle$ but statistically identical, because n_1 and h_2 are uncorrelated in the same way

as n_1 and n_2 . (To simplify, we assume that there are no correlated sources of noise such as seismic activity).

The two terms appearing in the signal S grow in different ways as the observation time T increases. The first term $\langle h_1, h_2 \rangle$ increases linearly with time T , because $h_1 = h_2$. The second term $\langle n_1, n_2 \rangle$ can be thought of as a random walk on a one-dimensional line, and so on the average it grows $\propto \sqrt{T}$. We will show in Section 3.3 that

$$\langle h_1, h_2 \rangle \propto |\tilde{h}(f)|^2 \Delta f T \propto \Omega(f) \Delta f T \quad (16)$$

$$\langle n_1, n_2 \rangle \propto |\tilde{n}(f)|^2 \sqrt{\Delta f T} \quad (17)$$

where f is the central frequency at which the detector is sensitive, Δf is the effective bandwidth, and \tilde{Q} is the Fourier transform of Q . Because the “signal” $\langle h_1, h_2 \rangle$ grows like T , and the noise $\langle n_1, n_2 \rangle$ only grows as $T^{1/2}$, with enough observation time one can in principle detect a gravitational wave stochastic background buried in any level of detector noise. Setting the “signal” term greater than the noise term gives a minimum detectable level of Ω :

$$\Omega_{\text{minimum detectable}} \propto \frac{|\tilde{n}(f)|^2}{\sqrt{\Delta f T}}. \quad (18)$$

Thus, even if the detector noise is much larger than the expected stochastic gravity wave strain, by making a long enough observation, one can in principle observe even very low levels of stochastic background.

Let me stress one more time that this crude analysis is intended primarily to present the concepts and basic ideas, and will be treated rigorously in Section 3.3.

3.2. The Overlap Reduction Function $\gamma(f)$

To provide a rigorous treatment of the signal analysis, we must take into account the reduction in sensitivity that results from two effects (1) the non-parallel alignment of the arms, and (2) the separation time delay between the two detectors. These two effects reduce the sensitivity of a stochastic background search; they mean that h_1 and h_2 are no longer equal; the overlap between the gravity wave strains in the two detectors is only partial.

To quantify these effects we introduce the *overlap reduction function* $\gamma(f)$ first calculated in closed form by Flanagan [16]. This is a dimensionless function of frequency f , which depends entirely on the relative positions and orientations of a pair of detectors. The overlap reduction function $\gamma(f)$ equals unity for co-aligned and coincident detectors, and decreases below unity when the detectors are rotated out of co-alignment (so they are sensitive to different polarizations) or shifted apart (so that there is a phase-shift between the signals in the two detectors). Later in these lectures (in Section 3.3) we will see how this function comes up naturally in the determination of signal-to-noise ratios.

The overlap reduction function is defined by [16]

$$\gamma(f) \equiv \frac{5}{8\pi} \int_{S^2} d\hat{\Omega} e^{2\pi i f \hat{\Omega} \cdot \Delta \vec{x}/c} (F_1^+ F_2^+ + F_1^\times F_2^\times). \quad (19)$$

Here $\hat{\Omega}$ is a unit-length vector on the two-sphere, $\Delta \vec{x}$ is the separation between the two detector sites, and $F_i^{+,\times}$ is the response of detector i to the + or \times polarization. For the first detector ($i = 1$) one has

$$F_1^{+,\times} = \frac{1}{2} (\hat{X}_1^a \hat{X}_1^b - \hat{Y}_1^a \hat{Y}_1^b) e_{ab}^{+,\times}(\hat{\Omega}), \quad (20)$$

where the directions of a single detector's arms are defined by \hat{X}_1^a and \hat{Y}_1^a , and $e_{ab}^{+,\times}(\hat{\Omega})$ are the spin-two polarization tensors for the “plus” and “cross” polarizations respectively. These quantities are defined in equations (A7,A8) of Appendix A.

It is not hard to see how the overlap reduction function $\gamma(f)$ arises. As we show in detail in Appendix A $\gamma(f)$ is proportional to the averaged product of the strains at two different detectors, when those detectors are driven by an isotropic unpolarized stochastic background of gravitational radiation at frequency f . This radiation is arriving at the detectors uniformly from all points on the celestial sphere, hence the integral over the direction $\hat{\Omega}$ of the wave-vector of the arriving radiation.

Let us look at each term in (19). (1) The overall normalization factor is chosen so that if $|\Delta \vec{x}| = 0$ (or equivalently, $f = 0$) and the two detectors are coincident, and the two detectors have parallel pairs of arms, then $\gamma \rightarrow 1$. (2) The exponential phase factor is the phase shift arising from the time delay between the two detectors for radiation arriving along the direction $\hat{\Omega}$. (3) The quantity F_1^+ is the response of the first detector to the “+” polarization wave, and similarly for detector 2 and the “cross” polarization.

In Section 3.3 this overlap reduction function will appear after a rigorous calculation; these remarks are meant primarily for motivation.

A graph of $\gamma(f)$ is shown in Fig. 5 for the two LIGO sites in Hanford, WA and Livingston LA. The overlap reduction function is *negative* as $f \rightarrow 0$. This is because, comparing the two LIGO sites, the arm orientations are not parallel but are rotated relative to one another by 90° . This can be seen immediately in Fig. 4. If the Livingston detector arms (denoted L2) were rotated by 90° in the clockwise direction, this would change the overall sign of $\gamma(f)$, but otherwise leave its dependence on f unchanged. The magnitude of $\gamma(0)$ is not unity, because the plane of the Hanford detector and that of the Livingston detector are different. Thus the arms of the two detectors are not exactly parallel, and hence $|\gamma(0)| = 0.89$ rather than 1.

The precise form of the overlap reduction function is not important here. However it can be calculated in closed form [16], and may be expressed as the sum of three Bessel functions:

$$\gamma(f) = A j_0(\alpha) + B \frac{j_1(\alpha)}{\alpha} + C \frac{j_2(\alpha)}{\alpha^2} \quad (21)$$

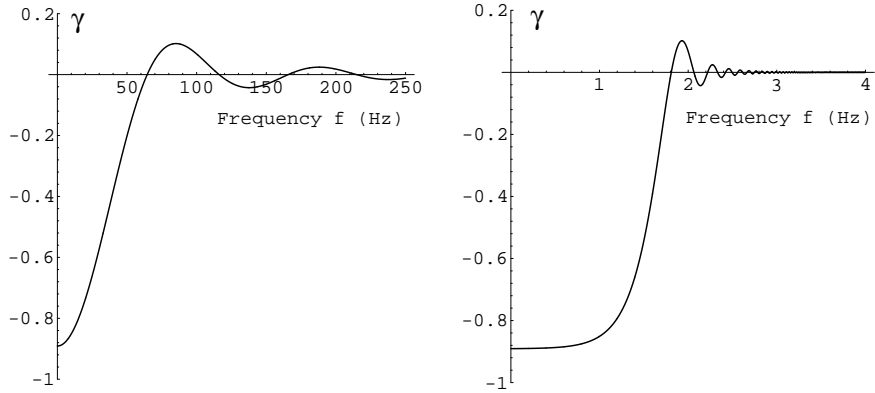


Fig. 5. — The overlap reduction function $\gamma(f)$ for the two LIGO detector sites. (The horizontal axis of the left-hand graph is linear, while that of the right-hand graph is \log_{10} .) The overlap reduction function shows how the correlation of the detector pair to an unpolarized stochastic background falls off with frequency. The overlap reduction function has its first zero at 64 Hz, as explained earlier. It falls off rapidly at higher frequencies.

where $\alpha = 2\pi f |\Delta\vec{x}|/c$ depends upon the detector separation and the frequency, and A, B, C are constants which only depend upon the locations of the detectors and the orientations of their arms [16].

3.3. Optimal Filtering

I now return to the subject that we addressed in Section 3.1: how do we detect a stochastic background? In this section, we work out the precise answer to this question. This type of analysis was first carried out by Michelson [14] then improved by Christensen [15] and further refined by Flanagan [16]. The analysis given here appears in Bayesian form in the work of Flanagan [16]; the treatment given here is the somewhat simpler “frequentist” version. The two different approaches yield exactly the same final results, because the signals are Gaussian.

Let us write the most general possible form of the correlation “signal” between two detectors in the form

$$S \equiv \int_{-T/2}^{T/2} dt \int_{-T/2}^{T/2} dt' s_1(t) s_2(t') Q(t - t'). \quad (22)$$

The strains s_1 and s_2 are the signal streams from (say) the Hanford and Livingston LIGO detectors, defined by (11-12), and $Q(t - t')$ is a real filter function. Because we are assuming that the statistical properties of our signals and noise are stationary, the “best choice” of filter function Q can only depend upon the

difference $\Delta t = t - t'$ of the two times. Our goal, in this section, is to find the *optimal choice* of filter function $Q(\Delta t)$ in a rigorous way.

The optimal choice of filter function $Q(\Delta t)$ depends upon the locations and orientations of the detectors, as well as on the spectrum of the stochastic background, and the noise characteristics of the detectors. If the two sites are very close together (compared to the characteristic wavelength at which the detectors are sensitive), have identical orientations, and the detectors have a narrow bandwidth, then the optimal choice of filter is a Dirac delta function $Q(t - t') = \delta(t - t')$. In this case, we just multiply the signals and integrate, precisely as discussed earlier in Section 3.1. Even if *none* of these assumptions holds, you will see that the optimal choice of filter function Q falls rapidly to zero for time delays Δt whose magnitude is large compared to the light travel time $d/c = 10^{-2}$ seconds between the two sites. We are thus justified in changing the limits above, to obtain

$$S = \int_{-T/2}^{T/2} dt \int_{-\infty}^{\infty} dt' s_1(t) s_2(t') Q(t - t'). \quad (23)$$

Since the observation time T will be at least several months, one can see immediately that the signal S gets most of its support in the integral (22) from the region near the diagonal line $t = t'$ in the region $[-T/2, T/2] \times [-T/2, T/2]$. Hence the value of S grows linearly with integration time T , in perfect agreement with the earlier “intuitive” explanation in Section 3.1.

The reader should note that with our definition, the “signal” S is a quantity *quadratic* in the strain h ; this is not the same as the convention frequently followed in analyzing signals from chirp or periodic sources, where the “signal” is generally taken to be a quantity *linear* in the strain h . For this reason, the expressions that we will derive for quantities such as the signal to noise ratio are in some ways analogous to the *squares* of the corresponding quantities for chirp or periodic signals.

We can re-write (23) in the frequency domain. Our convention for Fourier transforms is

$$\tilde{g}(f) = \int_{-\infty}^{\infty} dt e^{-2\pi i f t} g(t). \quad (24)$$

Here, and elsewhere in these lectures, * denotes complex conjugation, and within this section one may assume that $s_i(t)$ vanishes at some very early time (say, before the detector was built) and at some very late time (say, after the detector is decommissioned) so that the Fourier transforms are well-defined. Because we have assumed that the filter function is real, $\tilde{Q}(-f) = \tilde{Q}^*(f)$. Identical reality conditions hold for the signals \tilde{s}_i , the strains \tilde{h}_i , and the detector noise \tilde{n}_i . Using the Fourier transform, we may write the signal (23) as

$$S = \int_{-\infty}^{\infty} df \int_{-\infty}^{\infty} df' \delta_T(f - f') \tilde{s}_1^*(f) \tilde{s}_2(f') \tilde{Q}(f'). \quad (25)$$

The function δ_T which appears on the r.h.s. of (25) is a “finite time” approximation to the Dirac delta function, defined by

$$\delta_T(f) \equiv \int_{-T/2}^{T/2} dt e^{-2\pi ift} = \frac{\sin(\pi fT)}{\pi f}, \quad (26)$$

which reduces to the Dirac δ -function $\delta(f)$ in the limit $T \rightarrow \infty$. Note however that for finite observation times T one has $\delta_T(0) = T$. We now consider the stochastic properties of the signal S . In order to find the optimal choice of the filter function, some additional assumptions are needed.

As discussed in detail earlier, we will assume that the stochastic background is isotropic, unpolarized, and Gaussian. Under these assumptions, the expectation value of the Fourier amplitudes of the strain signal and the strain noise are derived in Appendix A:

$$\langle \tilde{h}_1^*(f) \tilde{h}_2(f') \rangle = \delta(f - f') \frac{3H_0^2}{20\pi^2} |f|^{-3} \Omega_{\text{gw}}(|f|) \gamma(|f|), \text{ and} \quad (27)$$

$$\langle \tilde{n}_i^*(f) \tilde{n}_j(f') \rangle = \frac{1}{2} \delta(f - f') \delta_{ij} P_i(|f|). \quad (28)$$

Here the indices i, j label the sites, so for example $i = 1$ is Washington and $i = 2$ is Hanford. The power spectral noise density function $P_i(f)$ which is defined by (28) is a real non-negative function, defined with a factor of 1/2 to agree with the standard definition used by instrument-builders, so that the total noise power is the integral of $P(f)$ over all frequencies from 0 to ∞ (rather than starting at $-\infty$). You will notice that we have assumed that the detector noise at the two different sites is completely uncorrelated. This assumption significantly simplifies the analysis, but is not entirely realistic [15, 16].

The predicted detector noise for the initial and advanced LIGO is shown in Fig. 6. This figure is taken from the LIGO design goals [1]. Because the 4 kilometer detectors are identical, they have the same power spectral noise densities, $P(f) = P_1(f) = P_2(f)$. There are at least three different sources of detector noise which dominate at different frequencies. At the low frequency end, the dominant source of noise is seismic noise. In the advanced version of LIGO, this noise will be reduced by improving the mechanical filters that isolate the detector from the ground. In the mid-band region, the noise is primarily due to thermal motion of the masses and mirrors, which will be reduced by using improved materials and design. In the high-frequency part of the spectrum, the noise is dominated by photon shot noise, which can be reduced by increasing the laser power and improving the optical components.

Although in the case of the LIGO detectors, the noise power spectra of the detectors are expected to be the same, in general, we are interested in correlating the outputs of detectors with different designs (say the LIGO and VIRGO detectors). So we will keep our treatment fairly general, and treat $P_1(f)$ and $P_2(f)$ as distinct functions.

In order to find the optimal choice of filter function Q , we need to choose the quantity to maximize. The natural choice here is to maximize the ratio

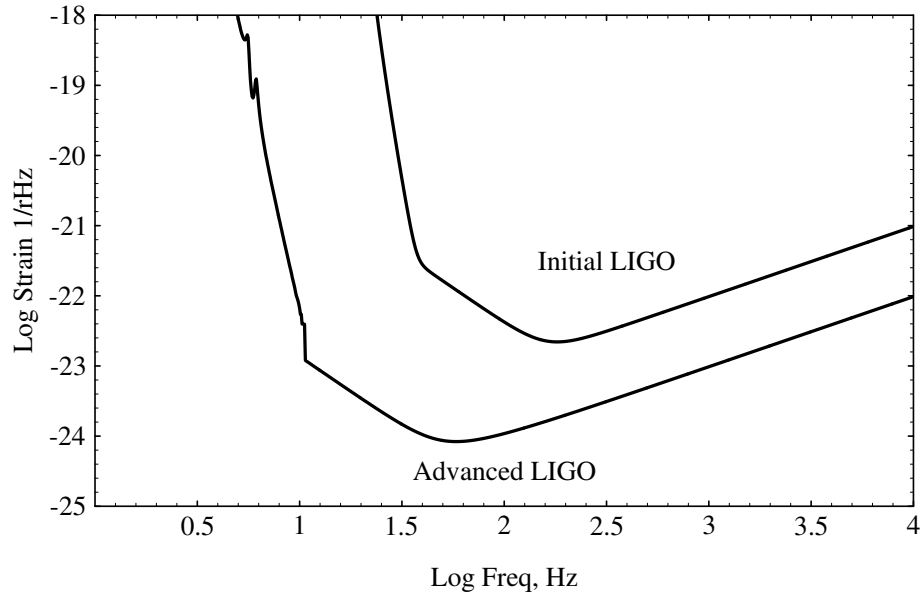


Fig. 6. — The predicted noise power spectra of the initial and advanced LIGO detectors. The horizontal axis is \log_{10} of frequency f , in Hz. The vertical axis shows $\log_{10}(P(f)/\text{sec})^{1/2}$, or strain per root Hz. These noise power spectra are the published design goals. The bumps appearing in the low-frequency part of the advanced LIGO noise curve are obtained by folding measured seismic noise data with the predicted transfer function of the seismic isolation (stack) system.

of signal-to-noise. The expected value of the signal is obtained by taking the expectation value of (25), making use of (27). Because the noise in each detector is uncorrelated with the other detector, and is uncorrelated with the gravity-wave strain h , one obtains

$$\langle S \rangle = \int_{-\infty}^{\infty} df \int_{-\infty}^{\infty} df' \delta_T(f - f') \langle \tilde{h}_1^*(f) \tilde{h}_2(f') \rangle \tilde{Q}(f') \quad (29)$$

$$= \frac{3H_0^2}{20\pi^2} T \int_{-\infty}^{\infty} df \gamma(|f|) |f|^{-3} \Omega_{\text{gw}}(|f|) \tilde{Q}(f). \quad (30)$$

The factor of T on the r.h.s. arises from evaluating $\delta_T(0)$. To determine the amount of noise N in the detector, we consider the variation of the signal S away from its mean value:

$$N \equiv S - \langle S \rangle. \quad (31)$$

The quantities on the r.h.s. are easily determined, if we assume as in (14) that the noise $n_i(t)$ each detector is much larger in magnitude than the gravitational

strain $h_i(t)$. In this case, one may simply replace the detector output signal (gravity strain + noise) by the detector noise alone in (25), obtaining

$$N \approx \int_{-\infty}^{\infty} df \int_{-\infty}^{\infty} df' \delta_T(f - f') \tilde{n}_1^*(f) \tilde{n}_2(f') \tilde{Q}(f'). \quad (32)$$

This approximation is consistent with the definition of N ; a brief calculation shows that the expected value of N vanishes, because the noise in the two detectors is assumed to be uncorrelated,

$$\langle N \rangle = 0, \quad (33)$$

a result which also follows directly from the definition of N . However the r.m.s. value of the expected noise is not zero, because if we take the expectation value of the square of (32) and use (28) one obtains

$$\langle N^2 \rangle = \langle S^2 \rangle - \langle S \rangle^2 \quad (34)$$

$$= \frac{1}{4} \int_{-\infty}^{\infty} df \int_{-\infty}^{\infty} df' \delta_T^2(f - f') P_1(|f|) P_2(|f'|) |\tilde{Q}(f')|^2. \quad (35)$$

For long observation times (say $T > 1$ sec) the finite-time delta function $\delta_T(f - f')$ is sharply peaked over a region in $f - f'$ whose size $\approx 1/T$ is very small compared to the scale on which the functions P_1, P_2, \tilde{Q} are changing. In this case we are justified in replacing one of the finite-time delta functions above by a Dirac delta function, obtaining

$$\langle N^2 \rangle = \frac{T}{4} \int_{-\infty}^{\infty} df P_1(|f|) P_2(|f|) |\tilde{Q}(f)|^2. \quad (36)$$

Notice that the expected r.m.s. noise $\langle N^2 \rangle^{\frac{1}{2}}$ grows as \sqrt{T} , in complete agreement with the simple intuitive explanation given earlier in Section 3.1.

The problem now is to find the choice of filter function \tilde{Q} which maximizes the signal to noise ratio

$$\left(\frac{S}{N} \right) \equiv \frac{\langle S \rangle}{\langle N^2 \rangle^{\frac{1}{2}}}. \quad (37)$$

This turns out to be remarkably straightforward, if we introduce an inner product between two functions of frequency, $A(f)$ and $B(f)$. This inner product takes as inputs two arbitrary complex functions $A(f)$ and $B(f)$; the output (A, B) is a single complex number. We define this inner product by

$$(A, B) \equiv \int_{-\infty}^{\infty} df A^*(f) B(f) P_1(|f|) P_2(|f|). \quad (38)$$

It is straightforward to see that this inner product is positive definite; since $0 < P_i(f)$ the norm of a function (A, A) vanishes if and only if $A(f)$ vanishes.

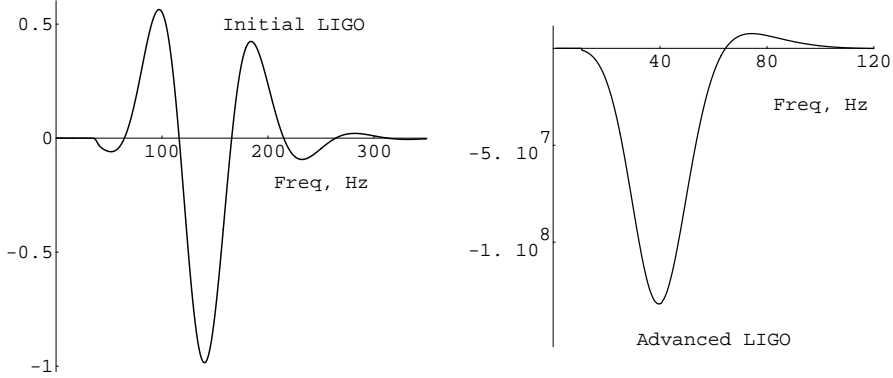


Fig. 7. — Optimal filter functions $\tilde{Q}(f)$ for the initial and advanced LIGO detectors, for $\Omega_{\text{gw}} = \text{constant}$. In this case $\tilde{Q}(f)$ is proportional to $\frac{\gamma(|f|)}{f^3 P^2(f)}$. The initial LIGO filter is normalized to have maximum magnitude of unity; the advanced LIGO filter is shown with an identical scale. It is much larger in magnitude because the power spectral noise density $P(f)$ of the advanced detectors is much smaller than in the initial detectors.

In terms of this inner product, we can express the expected signal and noise as

$$\langle S \rangle = (\tilde{Q}, \frac{\gamma(|f|)\Omega_{\text{gw}}(|f|)}{|f|^3 P_1(|f|)P_2(|f|)}) \frac{3H_0^2}{20\pi^2} T, \text{ and} \quad (39)$$

$$\langle N^2 \rangle = \frac{1}{4}(\tilde{Q}, \tilde{Q}) T. \quad (40)$$

So the problem is to choose the function \tilde{Q} which gives the largest possible value of

$$\left(\frac{S}{N} \right)^2 = \frac{\langle S \rangle^2}{\langle N^2 \rangle} = \left(\frac{3H_0^2}{10\pi^2} \right)^2 T \frac{(\tilde{Q}, \frac{\gamma(|f|)\Omega_{\text{gw}}(|f|)}{|f|^3 P_1(|f|)P_2(|f|)})^2}{(\tilde{Q}, \tilde{Q})}. \quad (41)$$

But this is trivial! Suppose you were given a fixed three-vector \vec{A} , and asked to find the three-vector \vec{Q} which maximized the ratio $\frac{(\vec{A}, \vec{Q})^2}{\vec{Q} \cdot \vec{Q}}$. Since this is just the squared cosine of the angle between the two vectors, the ratio is obviously maximized by choosing \vec{A} and \vec{Q} to point in the same direction! The problem of maximizing (41) is identical; the solution is to choose

$$\tilde{Q}(f) = \frac{\gamma(|f|)\Omega_{\text{gw}}(|f|)}{|f|^3 P_1(|f|)P_2(|f|)}. \quad (42)$$

Of course the overall constant appearing in the normalization of Q has no significance, since it does not affect the signal-to-noise ratio (41). We have now found the form of the optimal filter for a stochastic background search.

These optimal filters are shown in Fig. 7 for both the initial and advanced LIGO detectors, for a flat spectrum $\Omega_{\text{gw}} = \text{constant}$. Effectively, the filter includes into the signal only those frequencies at which the detector is most sensitive, weighting each frequency by a positive or negative factor which reflects the relative phasing (at that frequency) of the signals at the two detectors.

Having now found the optimal choice of filter function, it is straightforward to calculate the signal-to-noise ratios for a given pair of detectors. Substituting the optimal choice of Q given by (42) into (41) gives the optimal signal-to-noise ratio:

$$\left(\frac{S}{N}\right)^2 = \frac{9H_0^4}{50\pi^4} T \int_0^\infty df \frac{\gamma^2(f)\Omega_{\text{gw}}^2(f)}{f^6 P_1(f)P_2(f)}. \quad (43)$$

Thus the signal-to-noise ratio of a correlation experiment to detect a stochastic gravitational wave background is determined by the following quantities.

$$\begin{aligned} H_0 &= \text{Hubble expansion rate, sec}^{-1}. \\ T &= \text{Integration time, sec.} \\ \gamma(f) &= \text{Overlap reduction function, dimensionless.} \\ \Omega_{\text{gw}} &= \text{Fractional energy density in gravitational waves.} \\ P_i &= \text{Noise power spectral density of detector } i \text{ (one sided), sec.} \end{aligned}$$

One of the curious things about this formula for the signal-to-noise ratio is that it depends upon the spectrum of gravitational waves Ω_{gw} ; a function which we do not know! What this means in practice is that rather than having a single “optimal filter” one needs to have a set of such filters. The bandwidth of the experiment is in a good sense defined by the factor $\frac{1}{P_1(f)P_2(f)}$ appearing in the integrand of (43); the bandwidth of the experiment is the range of frequencies over which this factor is large (and hence the noise is small). The signal-to-noise ratio gets its significant contributions from within this bandwidth. Within this range of frequencies, which will not be very wide for the first generation of detectors, it is reasonable to assume that the form of the Ω_{gw} is a power-law, proportional to f^α . Thus, one can construct a reasonable set of optimal filters by choosing a number of different values of α such as $\alpha = -4, -7/2, \dots, 7/2, 4$ and analyzing the signal separately for each filter. The filter for $\alpha = 0$ is shown in Fig. 7.

In the next section, we will look at the values of this signal-to-noise ratio for the forthcoming detectors, and estimate the detectable levels of Ω_{gw} .

3.4. Signal to Noise Ratios, and the Minimum Detectable Ω_{gw}

One can see from (25) that in a measurement over the time interval T the signal S is a sum (over f and f') of many independent random variables (the Fourier amplitudes of the signals). This is because the amplitudes $\tilde{s}_1(f)$ and $\tilde{s}_1(f')$ are only correlated when $|f - f'| < 1/T \approx 10^{-7}$ Hz, and the bandwidth over which the integral in (25) gets its major contribution is ≈ 100 Hz wide. Thus S is the

sum of $\approx 10^9$ random variables, and the value of S in a set of measurements over independent time intervals is a Gaussian random variable. If the signal S is measured many times, each time over a distinct period of length T , the values of S will have a Gaussian normal distribution. The mean value of this distribution is $\langle S \rangle$; the width or standard deviation of this distribution away from its mean value is $\langle N^2 \rangle^{\frac{1}{2}}$.

In order to reliably detect a stochastic background, we need to be able to state, with some certainty, that the value of Ω_{gw} is greater than zero. Equivalently, one needs to be able to state with some desired reliability that the observed positive mean value of S could not have resulted from detector noise but instead must have resulted from a stochastic background.

One way of doing this is to compute the probability that a random variable with a Gaussian normal distribution will lie within a given range. For example, the probability that a Gaussian random variable S with mean $\langle S \rangle$ and variance² $= \langle N^2 \rangle$ will lie within the range $[S_l, S_u]$ is

$$\text{Probability} = \frac{1}{\sqrt{2\pi\langle N^2 \rangle}} \int_{S_l}^{S_u} dx \exp\left(\frac{-(x - \langle S \rangle)^2}{2\langle N^2 \rangle}\right). \quad (44)$$

This integral can be expressed in closed form in terms of the error function Erf. In this way, one can easily show that

$$\begin{aligned} \text{with 68\% probability} \quad S &\in [\langle S \rangle - \sqrt{\langle N^2 \rangle}, \langle S \rangle + \sqrt{\langle N^2 \rangle}] \\ \text{with 90\% probability} \quad S &\in [\langle S \rangle - 1.65\sqrt{\langle N^2 \rangle}, \langle S \rangle + 1.65\sqrt{\langle N^2 \rangle}] \\ \text{with 95\% probability} \quad S &\in [\langle S \rangle - 2\sqrt{\langle N^2 \rangle}, \langle S \rangle + 2\sqrt{\langle N^2 \rangle}] \\ \text{with 99.7\% probability} \quad S &\in [\langle S \rangle - 3\sqrt{\langle N^2 \rangle}, \langle S \rangle + 3\sqrt{\langle N^2 \rangle}]. \end{aligned}$$

Thus, to detect a stochastic background with $\geq 90\%$ confidence, we need to ensure that the signal-to-noise ratio $(\frac{S}{N}) \geq 1.65$, so that there is less than a ten percent probability that S is less than 0.

As an example, let's analyze the sensitivity of the first and second generation of LIGO detectors, to a flat spectrum $\Omega_{\text{gw}} \propto f^0$. The design goals [1] for the noise power spectral densities of the detectors are shown in Fig. 6. The minimum flat spectral density detectable in $T = 4$ months of integration, with 90% confidence, is given by

$$\Omega_{\text{gw}}^{\text{90\% confidence}} = 1.65 \left[\frac{9H_0^4}{50\pi^4} T \int_0^\infty df \frac{\gamma^2(f)}{f^6 P_1(f) P_2(f)} \right]^{-\frac{1}{2}} \quad (45)$$

$$= 5 \times 10^{-6} h_{100}^{-2} \text{ for initial LIGO} \quad (46)$$

$$= 5 \times 10^{-11} h_{100}^{-2} \text{ for advanced LIGO.} \quad (47)$$

We will see in the coming lectures that this is a very useful level of sensitivity, particularly for the advanced detectors.

One might wonder why the upgrade from the initial LIGO detectors to the advanced detectors results in such a large increase in sensitivity. The reason

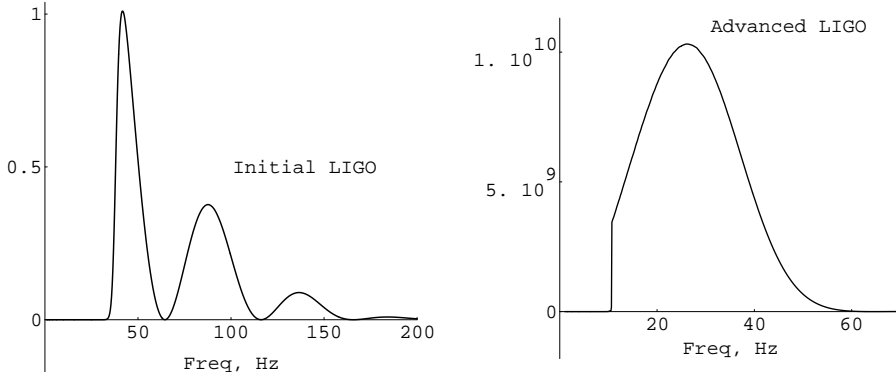


Fig. 8. — The expected “signal” as a function of frequency for a flat spectrum $\Omega_{\text{gw}} = \text{constant}$ in the initial and advanced LIGO detectors. The function displayed here is the integrand of Eqn. (30); it is proportional to $\frac{\gamma^2(f)}{f^6 P^2(f)}$. The initial LIGO signal is normalized to have maximum magnitude of unity; the advanced LIGO signal is shown with an identical scale. It is much larger in magnitude because the power spectral noise density of the advanced detectors is much smaller than in the initial detectors.

can be easily seen by comparing the optimal filter functions $\tilde{Q}(f)$ in for the initial and advanced detectors shown in Fig. 7, and the expected contributions to $\langle S \rangle$ given by (30), as a function of frequency, shown in Fig. 8. It is easy to see that because the advanced version of the LIGO detector will have much less low-frequency noise than the initial detector, the expected signal in the LIGO detector lies within the $0 < f < 64$ Hz region where the overlap reduction function $\gamma(f)$ has the greatest magnitude.

4. What Is Known (Experimental/Observational Facts) About The Stochastic Background?

So far in these lectures, we have discussed notation which may be used to describe the spectrum of a stochastic gravitational wave background, and some of the expected properties that such a background might have. We also discussed, in detail, the optimal way correlate the output of two interferometers to search for such a background.

In this section, I’d like to show you what is actually known about the stochastic background: the observational facts. As you will see, there are strict limits on the stochastic background in only a couple of frequency ranges, but other than that, only one very general constraint. In particular, there are really no strong constraints on Ω in the frequency range of interest for ground based interferometric experiments or bar detectors ($1 \text{ Hz} < f < 10^3 \text{ Hz}$) or space-based experiments ($10^{-4} \text{ Hz} < f < 10^{-1} \text{ Hz}$).

4.1. CMBR isotropy and the gravitational stochastic background

The strongest constraint on Ω comes from the high degree of isotropy observed in the Cosmic Microwave Background Radiation (CMBR). In particular, the one-year [22, 23, 24] and two-year data-sets [25] from the Cosmic Background Explorer (COBE) satellite place very strong restrictions on Ω at very low frequencies. The four-year data has also appeared, although it is not yet in print [26].

The temperature fluctuation δT of the CMBR away from its mean value of $T = 2.73$ K varies from point to point on the sky, and may be expanded in harmonic functions on the celestial sphere:

$$\frac{\delta T}{T}(\hat{\Omega}) = \sum_{lm} a_{lm} Y_{lm}(\hat{\Omega}). \quad (48)$$

Here $\hat{\Omega}$ denotes a point on the two-sphere, and the $a_{l,m}$ are the multipole moments of the CMBR. Since by definition the mean value of the l.h.s. vanishes, the sum begins at $l = 1$:

$$\sum_{lm} \equiv \sum_{l=1}^{\infty} \sum_{m=-l}^l. \quad (49)$$

The COBE data permitted a determination of the rms quadrupole moment of these fluctuations,

$$Q_{\text{rms}} \equiv T \sqrt{\sum_{m=-2}^2 \frac{|a_{2,m}|^2}{4\pi}} = 14.3_{-3.3}^{+5.2} \mu\text{K}. \quad (50)$$

These in turn place rather tight constraints on the spectrum of gravitational radiation at very long wavelengths.

The connection between the temperature fluctuations of the CMBR and gravitational waves arises through the *Sachs Wolfe effect*. In 1967 Sachs and Wolfe [27] showed how variations in the density of the cosmological fluid and gravitational wave perturbations result in CMBR temperature fluctuations, even if the surface of last scattering was perfectly uniform in temperature. In particular, they showed that to lowest order the temperature perturbation at a particular point on the sky is given by

$$\frac{\delta T}{T}(\hat{\Omega}) = \frac{1}{2} \int_{\text{null geodesic}} d\lambda \frac{\partial}{\partial \eta} h_{rr}. \quad (51)$$

Here the integral is taken over a null geodesic path which leaves our current spacetime point heading off in the spatial direction defined by $\hat{\Omega}$ and going back to the surface of last scattering of the CMBR, and λ is a particular choice of affine parameter along that null geodesic. In conformal coordinates the metric perturbation is given by $\delta g_{ij} = a^2(\eta)h_{ij}$, and r is a outwards radial spatial

Table I. — Two of the millisecond pulsars studied by Taylor's group, and then used to place limits on the stochastic gravitational wave background.

Pulsar Name	Time Observed t	Period	Timing Residuals Δt
PSR B1855+09	7 Years	5.4 msec	no residuals
PSR B1937+21	8 Years	1.6 msec	few μ sec (total)

coordinate from our current spacetime point. The effect of a long wavelength gravitational wave is to shift the temperature distribution of the CMBR on the celestial sphere away from perfect isotropy. The fact that the temperature perturbations are quite small (a few parts in 10^6) implies that the perturbations caused by the gravitational waves can not be too large. (One specific example of this effect can be found in [28, 29]. In those papers, we give a rigorous calculation of the effects of a stochastic gravity-wave background on the CMBR temperature distribution, in an inflationary model of the early universe.)

If we combine the COBE observational limits on the different multipole moments ($2 \leq l \leq 30$) we arrive at the constraint on Ω_{gw} given by

$$\Omega_{\text{gw}} h_{100}^2 < 7 \times 10^{-11} \left(\frac{H_0}{f} \right)^2 \quad \text{for } H_0 < f < 30H_0. \quad (52)$$

Note that this limit does not apply to *any* gravitational waves, but only to those of cosmological origin, which were already present at the time of last scattering of the CMBR. This limit applies only over a narrow band of frequencies at the very lowest limits of Fig. 1; it is far below an frequencies that will be accessible to investigation either by space-based or earth-based experiments.

In the Section 5.1 we will make a detailed examination of inflationary cosmological models, and investigate these limits on Ω_{gw} in more detail.

4.2. Millisecond Pulsar Timing Constraints on Ω_{gw}

For about a decade, Taylor and his research group [30] have been monitoring the radio pulses arriving from a number of stable millisecond pulsars. Two of these pulsars are described in Table I. These objects have turned out to be remarkably stable clocks; the regularity of their pulses places tight constraints on Ω_{gw} at frequencies of order $1/\text{observation time} \approx 10^{-8}\text{Hz}$.

The regularity of these pulsar's pulses can be described in terms of *timing residuals*. Roughly speaking, after fitting the arrival times of the pulses to a uniformly-spaced set (in the rest frame of the pulsars) the timing residuals are the remaining errors in the emission times of the pulses. As can be seen from Table I the timing residuals are remarkably small; in dimensionless terms,

$$\frac{\Delta t}{t} \approx \frac{\mu\text{sec}}{8 \text{ years}} < 10^{-14}. \quad (53)$$

It is easy to see that these extremely precise measurements put very tight restrictions on the amplitude of any gravitational waves with periods comparable to 8 years.

To see the exact connection, imagine that a gravitational wave is passing by us, coming from a direction transverse to our line-of-sight to the pulsar, and assume its wavelength is 8 light years. Assume in addition that the pulsar is an ideal clock, emitting pulses at perfectly regular intervals in its rest frame. Then, during the time when one of the maxima of the gravitational wave is passing by the earth, the pulsar pulses will arrive spaced slightly farther *apart* (you can think of this as gravitational redshifting due to the gravitational wave). Four years later, a minimum of the gravitational wave will be passing by the earth, and the pulsar pulses arrive at an earth-bound observer slightly more closely spaced *together* (which can be thought of as gravitational blueshifting). In fact this system is just like a single-arm gravitational wave detector, with an arm length L of 8 light years. The size of the characteristic gravity-wave strain must be less than of order

$$h_c \leq \Delta L/L = \Delta t/t \leq 10^{-14}, \quad (54)$$

where $L = t = 8$ years and $\Delta t \approx \mu\text{sec}$ is an upper bound on the residual timing error. Substituting $f = (8 \text{ years})^{-1} = 10^{-8} \text{ Hz}$ in Eqn. (9) gives the relation $h_c = 10^{-10} \sqrt{\Omega(f = 10^{-8} \text{ Hz})}$ between the characteristic strain and the fractional energy density in gravitational waves. Hence the extremely small size of the fractional timing errors restricts h_c to be extremely small, which in turn gives a bound on Ω of

$$\Omega(f = 10^{-8} \text{ Hz}) < 10^{-8}. \quad (55)$$

This bound provides important constraints on cosmic string networks, as discussed in more detail in Section 5.2. However it is not directly relevant for LIGO and other ground-based detectors, because the bound is at a frequency 10 orders of magnitude lower than their band of observation frequencies.

The sensitivity of these pulsar timing experiments is truly remarkable! For example, the authors point out that in their 7-year data set for pulsar PSR B1855+09, the pulsar rotated precisely 40,879,349,533 times on its axis! They also conclude that remaining timing residuals are not due to gravitational waves: “We do not consider it likely that the observed trends in the timing residuals are in fact caused by gravity waves.”

I should note that a re-analysis of this pulsar timing data has recently appeared [31], which gives even more stringent limits (at 90% confidence) of $\Omega_{\text{gw}} < 4.8 \times 10^{-9}$ at 4.4×10^{-9} Hz. However this analysis has been criticized in other work [32] which uses a different method (Bayesian rather than frequentist Neyman-Pearson tests) to analyze the data, so it is still not entirely certain that the more stringent limit is reliable.

4.3. Nucleosynthesis limits on Ω_{gw}

The final bound on Ω is obtained from the standard model of big-bang nucleosynthesis (often referred to as BBN [17]). This model provides remarkably accurate fits to the observed abundances of the light elements in the universe, tightly constraining a number of key cosmological parameters. One of the parameters which is constrained in this way is the expansion rate of the universe at the time of nucleosynthesis. This in turn places a constraint on the energy-density of the universe at that time, which in turn constrains the energy-density in a cosmological background of gravitational radiation.

The BBN model's constraint can be expressed in terms of the number of massless neutrinos, which can be present and in thermal equilibrium at the time of nucleosynthesis. One typically obtains a bound of the form [17]

$$\int d(\ln f) \Omega_{\text{gw}} \text{ at nucleosynthesis} \leq \frac{\frac{7}{8}(N_\nu - 3)}{1 + 3 \times \frac{7}{8} + 2 \times \frac{7}{8}} \left(\frac{\rho_{\text{rad}}}{\rho_{\text{crit}}} \right) \text{ at nucleosynthesis} \quad (56)$$

where the quantities appearing on each side are the fractional energy densities in gravitational radiation and in relativistic matter *at the time of nucleosynthesis*. The BBN model constraints can be expressed in terms of the number of massless neutrinos permitted; this is $N_\nu \leq 3.4$. To give a rough idea of the limits on the present-day spectrum of Ω_{gw} , we can convert this limit at the time of nucleosynthesis to a limit today. Since the energy-density of radiation (relative to the dominant energy density in the universe) redshifts $\propto (1 + Z)^{-1}$ after the time of equal matter and radiation energy densities, this inserts a factor of $(1 + Z)^{-1}$ into the limits. One obtains a bound on Ω_{gw} today of

$$\int \Omega_{\text{gw}} d(\ln f) \leq 0.07 \times (1 + Z_{\text{eq}})^{-1} \approx 10^{-5}, \quad (57)$$

where $Z_{\text{eq}} \approx 6000$ is the redshift at the time of equal matter and radiation energy densities. This bound restricts the spectrum of gravitational radiation Ω_{gw} at all frequencies, but is not a very restrictive constraint.

5. Cosmological Sources of a Stochastic Background

In this section, we will examine in detail three different physical processes which might have taken place in the early universe, which give rise to different spectra of Ω_{gw} . In addition to their general interest, these three examples serve to motivate a number of interesting observations and comments.

The first model we examine is the standard “inflationary” scenario for the early universe [17, 33]. In this model, as the universe cooled, it passed through a phase in which the energy-density of the universe was dominated by vacuum energy, and the scale factor increased exponentially-rapidly. You will see that in its simplest version, this scenario is tightly constrained by the CMBR

observational data [28, 29]. When this constraint is taken into account, the stochastic gravity wave background predicted by the simplest inflationary cosmological models are far too weak to be observable by either the initial or advanced LIGO detectors.

The second model we examine is the cosmic string scenario [34, 35]. In this model, as the universe cooled, long stringlike defects were formed at a phase transition. These “cosmic strings” form a network which self-intersects and chops off small loops of string. These small loops oscillate relativistically, and as they do so they emit a characteristic spectrum of gravitational waves. In contrast with the previous example, for reasonable values of the parameters, the cosmic string scenario predicts a stochastic background which is large enough to be observable with the advanced LIGO detector. In common with the previous example, the string network is described by a “scaling” solution, with the consequence that the spectrum of Ω_{gw} is flat over a wide range of frequencies.

The third and final example in this section is also motivated by a phase transition in the early universe. We consider the case in which the phase transition is strongly first-order, and creates vacuum bubbles, which are bubbles of the new (low energy density) phase expanding in the old (high energy density) phase [36, 37, 38]. Within a short time, these bubble walls are moving relativistically, and much of the latent energy released by the phase transition is transformed into kinetic energy of the bubble walls. The highly-relativistic collisions of these bubble walls are a copious source of gravitational radiation, strong enough to be observable (in some cases) with the initial generation of LIGO detectors. Unlike the previous two examples, this phase transition/gravitational radiation production process is a “one-time” event, characterized by a particular cosmological time and a particular frequency today. Hence, in contrast with the previous two examples, you will see that the spectrum $\Omega_{\text{gw}}(f)$ is strongly peaked at a frequency characteristic of this time.

These three examples are intended primarily to be illustrative. They are by no means comprehensive. The fact of the matter is that we don’t know what happened in the early universe – the subject is extremely speculative, and will remain so until we have data (such as the spectrum of Ω_{gw}) that carries specific information about very early times. Nevertheless, these examples are quite useful, because they illustrate some of the mechanisms that might produce a cosmological stochastic background. They certainly lead me to suspect that such a background is present, and to hope that it might be observable.

5.1. Inflationary Cosmological Models

Inflationary models of the early universe were studied extensively in the early- and mid-1980’s (for a review, see [33]). Generally speaking, these are a class of cosmological models in which the universe undergoes a phase of very rapid (power-law or exponential in time) expansion at early times. Inflationary models have a number of nice properties. They are very simple, and highly predictive. They provide “natural” solutions to the horizon, flatness, and monopole

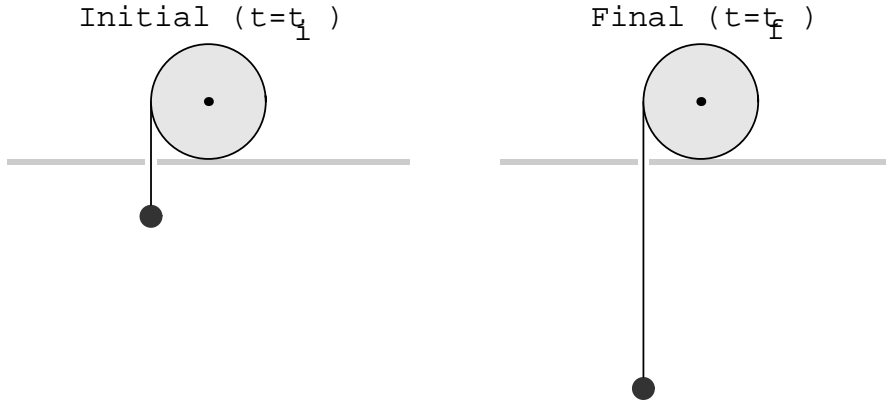


Fig. 9. — The pendulum consists of a mass hanging from a string. Initially the string is short, and the oscillation frequency is large. Between initial and final times t_i and t_f , the string is reeled out, increasing its length and decreasing the oscillation frequency of the mass. The quantum mechanical behavior of this system is more interesting than its classical behavior, and provides a simple model for the mechanism that generates large classical perturbations from zero-point fluctuations in inflationary cosmological models.

problems. They are also in good agreement with the COBE observations of the spectrum of temperature perturbations in the CMBR. (Note, however, that many other types of early-universe models are also in good agreement with these observations!)

One of the remarkable facts about inflationary models is that they contain a beautiful mechanism which creates perturbations in all fields. These provide, within the context of inflationary models, a natural mechanism to create the density perturbations which evolved to form galaxies and clusters of galaxies today. More important for our purposes is that this mechanism also gives rise to an extremely distinctive spectrum of stochastic gravitational radiation.

In this lecture, I will show you how these perturbations in inflationary cosmologies arise from the most basic quantum mechanical effect: the uncertainty principle. In effect, the spectrum of gravitational radiation that might be observed today is nothing other than adiabatically-amplified zero-point fluctuations.

Let me begin with a simple example. Suppose that we have a harmonic oscillator like the one shown in Fig. 9. It is a traditional pendulum, consisting of a mass on a string. In this case however the string is wound around a reel, and by unwinding the reel one can increase the length of the string and decrease the oscillation frequency $\omega = \sqrt{g/l}$ of the system. Here l is the length of the string and g is the acceleration of gravity at the surface of the earth. We will denote the initial frequency by $\omega_i = \sqrt{g/l_i}$ and the final frequency by

$\omega_f = \sqrt{g/l_f}$. Let us suppose that the mass is initially at rest in its equilibrium position and consider in turn its classical and its quantum behavior.

The *classical* behavior of this system is not very exciting. Since the mass is at rest in its minimum energy configuration (hanging straight down) it simply remains there. After reeling out the string, and lowering the frequency of the oscillator, the mass remains at rest, hanging straight down.

The *quantum mechanical* behavior of this system is far more interesting. It has a long history (neatly encapsulated as the “adiabatic theorem”) dating back to the invention of quantum mechanics in the 1920’s. Because of the uncertainty principle, it is impossible for the oscillator to be truly at rest; in the minimum energy state it has initial energy $E_i = \frac{1}{2}\hbar\omega_i$, and executes zero-point motion about its classical rest position. In this initial state, the initial number of quanta $N_i = 0$. Quantum mechanically, this system has two possible types of behavior, depending upon how the string is reeled out. To distinguish these two cases, let $T = t_f - t_i$ denote the time over which the string was steadily reeled out.

The case where T is quite long compared to both the initial and final oscillation periods, $T \gg 2\pi/\omega_f$, is the slow or adiabatic case. In this case, the final energy of the oscillator is $E_f = \frac{1}{2}\hbar\omega_f$. The difference between this energy and the initial energy represents work done to the reel that lowered the string. In addition to the “classical” work mgh done to the friction mechanism of the reel, a bit of additional “quantum” work $E_i - E_f$ is also done. In this case, no quanta are created, $N_f = 0$ and the mass is still in its ground state after being lowered down.

The truly fascinating case is the one in which T is quite short compared to the oscillation periods, $T \ll 2\pi/\omega_i$. (Strictly speaking, we need $\dot{l}/l > \omega$ at every moment.) In this case, the behavior of this quantum mechanical oscillator is quite different than the behavior of the corresponding classical oscillator. In this case, as I will shortly show you, the final energy is *half* of the initial energy: $E_f = \frac{1}{2}E_i = \frac{1}{4}\hbar\omega_i$. In this case, we create quanta: $N_f = \frac{1}{4}\frac{\omega_i}{\omega_f}$. It is in this way that the inflationary universe models create large macroscopic fluctuations today, starting only with the minimum fluctuations expected from the uncertainty principle. In order to solve the horizon and flatness problems, inflationary models require the universe to expand by a factor greater than $\approx 10^{27}$. This redshifts frequencies by the same amount, so that the ratio $\frac{\omega_i}{\omega_f} > 10^{27}$ and one ends up with large occupation numbers at the present.

Before going into the details of inflation, let me show you a simple calculation to justify and explain the claims made in the previous paragraph. Shown in Fig. 10 are the initial and final potentials of the harmonic oscillator pictured previously in Fig. 9. Let $\alpha_i = m\omega_i/\hbar$ where m is the mass of the ball. The initial wavefunction corresponding to the ground state is

$$\psi(x) = \left(\frac{\alpha_i}{\pi}\right)^{1/4} e^{-\frac{\alpha_i}{2}x^2}. \quad (58)$$

Imagine now that at time $t = 0$ this potential is suddenly changed to a final

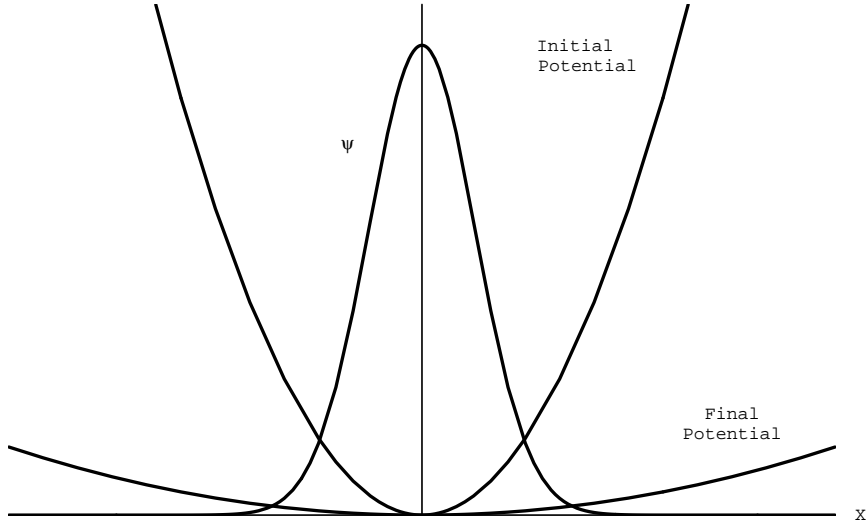


Fig. 10. — A particle moving in the initial harmonic oscillator potential is in the ground state, and has a wavefunction shown by $\psi(x)$. The frequency of the oscillator is suddenly decreased, by external means, and the potential becomes that shown as the final potential. The wavefunction no longer corresponds to the ground state, but to a highly-excited many-particle state.

potential which is another harmonic oscillator potential but with much lower frequency ω_f , as shown in Fig. 10. Let $\alpha_f = m\omega_f/\hbar$. Then we can express the wavefunction at time $t = 0$ in terms of the energy eigenstates of the new harmonic oscillator potential:

$$\psi(x) = \sum_{n=0}^{\infty} c_n \psi_n(x) \quad (59)$$

where $\psi_n(x)$ are the energy eigenfunctions of the final (lower frequency) potential:

$$\psi_n(x) = N_n H_n(\sqrt{\alpha_f} x) e^{-\frac{\alpha_f}{2} x^2}. \quad (60)$$

Here N_n is a normalization constant, and the H_n are Hermite polynomials. In the usual way, we can work out the values of the expansion coefficients c_n : we multiply both sides of (59) by $\psi_m^*(x)$ and integrate over all x , using the orthogonality of the eigenfunctions to obtain a formula for c_m :

$$c_n = 0 \text{ for } n \text{ odd, and} \quad (61)$$

$$c_{2n} = (\alpha_i \alpha_f)^{1/4} \sqrt{\frac{2(2n)!}{\alpha_i + \alpha_f}} \frac{1}{n!} \left(\frac{\omega_f - \omega_i}{2(\omega_f + \omega_i)} \right)^n \quad (62)$$

Table II. — The cosmological scale factor $a(\eta)$ for a simple two-stage inflationary cosmological model.

Time	Phase	Equation of State	Scale Factor $a(\eta)$	Hubble $H(\eta)$
$\eta < \eta_1$	DeSitter	$-P = \rho = \text{const.}$	$\eta_1^2 \eta_0^{-1} (2\eta_1 - \eta)^{-1}$	$H_{\text{ds}} = c\eta_0/\eta_1^2$
$\eta > \eta_1$	Radiation	$P = \rho/3$	η/η_0	$c\eta_0/\eta^2$

It is now straightforward to calculate the expectation value of the energy:

$$E_f = \sum_{n=0}^{\infty} (2n + 1/2) \hbar \omega_f |c_{2n}|^2 = \hbar \omega_f \left(\frac{1}{2} + \frac{(\omega_f - \omega_i)^2}{4\omega_i \omega_f} \right). \quad (63)$$

It is easy to see that in the limit when the final frequency is much lower than the initial frequency, $\omega_f \ll \omega_i$, one obtains $E_f \approx \frac{1}{4} \hbar \omega_i = \hbar \omega_f \left(\frac{1}{4} \frac{\omega_i}{\omega_f} \right)$. This allows us to identify the number of created quanta as $N_f = \left(\frac{1}{4} \frac{\omega_i}{\omega_f} \right)$.

This simple mechanical model shows exactly how inflationary models generate perturbations in a “natural” way. Every mode of every quantum field can be thought of as a simple harmonic oscillator, and when the universe expands exponentially rapidly in size, the frequencies of these modes drop extremely rapidly. As you will see shortly, in inflationary models, the universe expands rapidly in size, and because this expansion is very quick, it is *not adiabatic*! In other words, it corresponds to our second case above, where quanta are created. Even though this process is strictly quantum mechanical, and the energy created is proportional to \hbar , the occupation numbers today are large, and these perturbations appear today to be large macroscopic fluctuations. In the case of the gravitational field itself, this process creates a characteristic spectrum of stochastic gravitational waves. Let me now sketch the calculation for a simple inflationary model. The details of this calculation can be found in [39].

We assume that the universe is described by a simple “two-stage” cosmology as shown in Fig. 11. The metric of spacetime is given by

$$ds^2 = a^2(\eta) (-d\eta^2 + d\vec{x}^2 + h_{ij}(\eta, \vec{x}) dx^i dx^j), \quad (64)$$

where the scale factor $a(\eta)$, the Hubble expansion rate $H(\eta)$ and the equation of state are given in Table II. (Note: η is a conformal time coordinate with units of length.) Note that although the expansion does not appear to be very rapid during the deSitter phase ($\eta < \eta_1$) this is because the scale factor $a(\eta)$ has been expressed in terms of a conformal time coordinate. When expressed in terms of physical or comoving time defined by $cdt = a(\eta)d\eta$ the scale factor is $\propto e^{H_{\text{ds}}t}$ during the deSitter phase, and $\propto t^{1/2}$ during the radiation-dominated phase. In order to solve the horizon and flatness problems, enough expansion is needed to ensure that $a(\eta_0)/a(\eta_1) > 10^{27}$ for GUT-scale inflation. So typically one has $\eta_0 > 10^{27} \eta_1$.

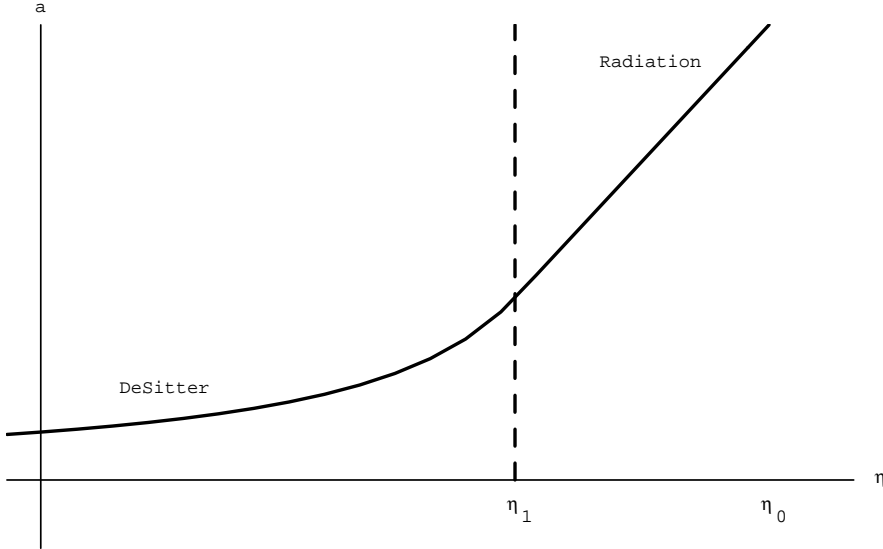


Fig. 11. — The cosmological scale factor $a(\eta)$ as a function of conformal time η , for a simple inflationary model. The universe is deSitter space until time $\eta = \eta_1$ when it makes an instantaneous phase transition to a radiation-dominated epoch. This would be a good “crude” model of our own universe, if slightly to the past of the present time η_0 the universe became matter-dominated and a increased somewhat more rapidly between that time and the present.

The gravitational waves in this simple two-stage cosmology are described by metric perturbations of the form [39]

$$h_{ij} = e_{ij}(\vec{k})\phi(\eta) \exp(i\vec{k} \cdot \vec{x}), \quad (65)$$

where \vec{k} is a constant (in time η) wavevector. The polarization tensors e_{ij} are given in equations (A7,A8) of Appendix A. The amplitude ϕ satisfies a wave equation (the massless Klein-Gordon equation [39])

$$\left(\frac{d^2}{d\eta^2} + \frac{2}{a} \frac{da}{d\eta} \frac{d}{d\eta} + |\vec{k}|^2 \right) \phi = 0. \quad (66)$$

The solutions to this wave equation may be easily found in terms of elementary functions (which are simple cases of half-integer Bessel or Hankel functions) in both the deSitter and radiation-dominated epochs:

$$\text{For } \eta < \eta_1 \quad \phi(\eta) = \frac{a(\eta_1)}{a(\eta)} [1 + iH_{\text{ds}}\omega^{-1}] e^{-ik(\eta-\eta_1)} \quad (67)$$

$$\text{For } \eta > \eta_1 \quad \phi(\eta) = \frac{a(\eta_1)}{a(\eta)} [\alpha e^{-ik(\eta-\eta_1)} + \beta e^{ik(\eta-\eta_1)}], \quad (68)$$

where $\omega = ck/a$ is the angular frequency of the wave, α and β are time-independent constants. Note that because $k = |\vec{k}|$ is constant, the angular frequency ω is a function of time. Since this differential equation is second order, one may obtain the values of the constants α and β by demanding that both ϕ and $d\phi/d\eta$ are continuous at the boundary $\eta = \eta_1$ between the deSitter and radiation epochs of expansion. Imposing this restriction on the solution leads to

$$\alpha = 1 + i \frac{\sqrt{H_0 H_{\text{ds}}}}{\omega} - \frac{H_0 H_{\text{ds}}}{2\omega^2} \quad (69)$$

$$\beta = \frac{H_0 H_{\text{ds}}}{2\omega^2}. \quad (70)$$

In these expressions, we use $\omega = ck/a(\eta_0)$ to denote the angular frequency that would be observed today, and $H_0 = c/\eta_0$ for the Hubble expansion rate that would be observed today. In effect, this problem is identical to tunneling problems done in elementary quantum mechanics, and we are simply calculating transmission/reflection coefficients. These types of calculations are also frequently referred to as Bogoliubov coefficient methods in the literature [40].

In an inflationary model, the long period of inflation damps out any classical or macroscopic perturbations, leaving behind only the minimum allowed level of fluctuation, required by the uncertainty principle. We have chosen our wave-function (67) to correspond precisely to this deSitter vacuum state. Provided that the period of inflation was long enough, the observable properties of the universe today should be indistinguishable from those of a universe which started in this vacuum state. We could work out the correct overall normalization of the wavefunction, but it is not necessary.

Today, in the radiation-dominated phase of the universe, the eigenmodes describing particles are the coefficients of α , and those describing antiparticles are the coefficients of β . One may easily show that the number of created particles of angular frequency ω today is given by [39, 40]

$$N_\omega \equiv \text{Number of created particles of freq } \omega = |\beta_\omega|^2 = \frac{H_0^2 H_{\text{ds}}^2}{4\omega^4}. \quad (71)$$

Along the lines of the calculation given in Section 2.1 and in particular in analogy with (1), we may write an expression for the stochastic gravitational-wave energy-density contained in the (angular) frequency interval $(\omega, \omega + d\omega)$ as

$$d\rho_{\text{gw}} = 2\hbar\omega \left(\frac{\omega^2 d\omega}{2\pi^2 c^3} \right) N_\omega = \frac{\hbar H_0^2 H_{\text{ds}}^2}{4\pi^2 c^3} \frac{d\omega}{\omega} = \frac{\hbar H_0^2 H_{\text{ds}}^2}{4\pi^2 c^3} \frac{df}{f}. \quad (72)$$

This may be re-written in terms of the present-day energy-density of the universe, and the (constant) energy-density during the deSitter phase, in the following way. The Hubble expansion rates are given in terms of these energy-densities by $H_0^2 = \frac{8\pi G \rho_c}{3c^2}$ and $H_{\text{ds}}^2 = \frac{8\pi G \rho_{\text{ds}}}{3c^2}$. The spectrum of stochastic

gravitational waves is thus

$$\Omega_{\text{gw}} = \frac{f}{\rho_c} \frac{d\rho_{\text{gw}}}{df} = \frac{16}{9} \frac{\hbar G^2}{c^7} \rho_{\text{ds}} = \frac{16}{9} \frac{\rho_{\text{ds}}}{\rho_{\text{Planck}}}, \quad (73)$$

where we have introduced the Planck energy density

$$\rho_{\text{Planck}} = \frac{c^7}{\hbar G^2} = 10^{115} \text{ ergs/cm}^3. \quad (74)$$

You will notice that Ω_{gw} is proportional to \hbar , because this background is nothing other than (parametrically-amplified) zero-point energy!

Several comments are now appropriate. First, our calculation of Ω_{gw} is for a simplified cosmological model that does not include a matter-dominated phase after the radiation-dominated epoch of expansion. If this matter-dominated phase is included, the result obtained is [39]

$$\Omega_{\text{gw}}(f) = \frac{16}{9} \frac{\rho_{\text{ds}}}{\rho_{\text{Planck}}} (1 + Z_{\text{eq}})^{-1}, \quad (75)$$

for those waves which, at the time the universe became matter-dominated, had a wavelength shorter than the Hubble length at that time. Today this corresponds to frequencies $f > (1 + Z_{\text{eq}})^{1/2} H_0$, where Z_{eq} is the redshift of the universe when the matter and radiation energy densities were equal. At lower frequencies, the spectrum of $\Omega_{\text{gw}}(f) \propto f^{-2}$. Second, note that our result (which is frequency-dependent) does not truly apply “from DC to light”. For waves which are long compared to the Hubble length (10^{28} cm today) corresponding to frequencies less than H_0 today, the notion of energy density becomes non-sensical, because the wavelength becomes longer than the curvature length scale of the background space-time. In similar fashion, at high frequencies there is a maximum frequency above which Ω_{gw} drops rapidly to zero. In our calculation, we assume that the phase transition from the deSitter to the radiation-dominated epoch is instantaneous. However this process occurs over some time scale $\Delta\tau$, and above a frequency

$$f_{\text{max}} = \frac{a(t_1)}{a(t_0)} \frac{1}{\Delta\tau} \quad (76)$$

which is just the redshifted characteristic rate of the transition, Ω_{gw} drops rapidly to zero. These low- and high-frequency cutoffs to the spectrum guarantee that the total energy-density in gravitational waves is finite rather than infinite.

A typical spectrum of gravitational waves resulting from inflation is shown in Fig. 12. For GUT energy-scale inflation, the ratio

$$\text{GUT - scale Inflation : } \frac{\rho_{\text{ds}}}{\rho_{\text{Planck}}} \approx (10^{16} \text{ GeV}/10^{19} \text{ GeV})^4 \approx 10^{-12}. \quad (77)$$

(Also shown for comparison is the naive 0.9 K blackbody, discussed in Section 2.1.) We have also chosen $f_{\text{max}} \approx 10^{10} \text{ Hz}$, a reasonable value for GUT-scale

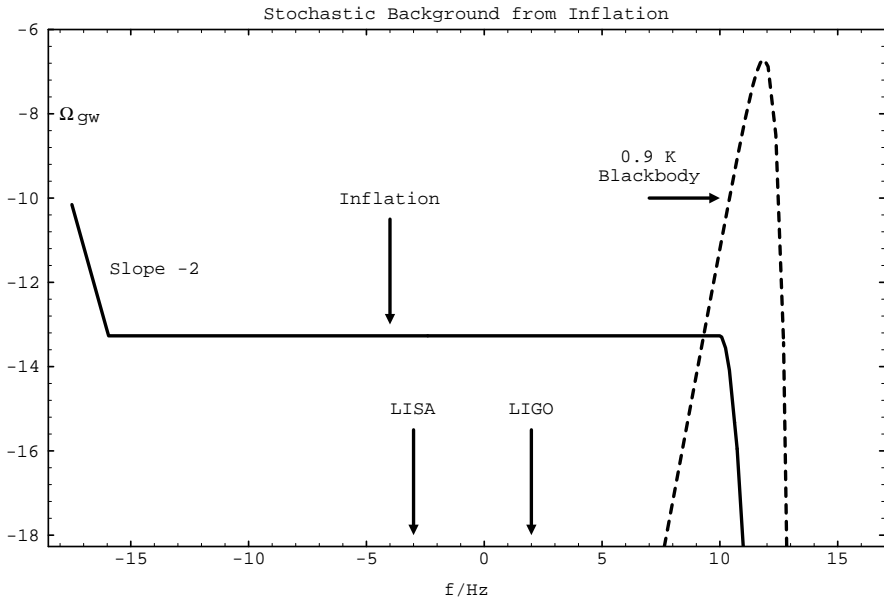


Fig. 12. — The spectrum of stochastic gravitational waves in inflationary models is flat over a wide range of frequencies, and is shown as the solid curve. The horizontal axis is \log_{10} of frequency, in Hz. The vertical axis is $\log_{10} \Omega_{\text{gw}}$. The inflationary spectrum rises rapidly at low frequencies (wave which re-entered the Hubble sphere after the universe became matter-dominated) and falls off above the (appropriately redshifted) frequency scale f_{max} associated with the fastest characteristic time of the phase transition at the end of inflation. The amplitude of the flat region depends only on the energy-density during the inflationary stage; we have chosen the largest amplitude consistent with the COBE constraint discussed earlier: $\Omega_{\text{gw}} < 7 \times 10^{-11}$ at 10^{-18} Hz. This means that at LIGO and LISA frequencies, $\Omega_{\text{gw}} < 8 \times 10^{-14}$. Shown for comparison is the spectrum of a 0.9 K blackbody, as discussed earlier.

inflation. You can see right away that in the inflationary case, the constraint coming from the COBE observations discussed in Section 4.1 puts very severe restrictions on the spectrum [28, 29]. In Fig. 12 we have chosen the amplitude of the spectrum (determined by the ratio $\frac{\rho_{\text{ds}}}{\rho_{\text{Planck}}}$) to be *as large as possible, consistent with this COBE constraint*. Nevertheless, because the spectrum falls off $\propto f^{-2}$ at low frequencies, this means that today, at LIGO and LISA frequencies (indicated by the arrows), $\Omega_{\text{gw}} < 8 \times 10^{-14}$. This is certainly too small to be observable with either initial or advanced LIGO, and is at the limits of what might be potentially observable with LISA.

Before moving on to our next example (cosmic strings) of how cosmological processes can give rise to a stochastic background, a few final comments are in order. The first is that the long flat region of the spectrum Ω_{gw} reflects the

scaling behavior of the cosmological scale factor $a(t) \propto \exp(H_{\text{dst}} t)$ during the deSitter phase of expansion. We will see identical self-similar behavior in our next example. Notice that the highest frequency parts of the spectrum (such as the falloff at 10^{10} Hz in our example) reflect the behavior of the universe at early times (in this example, the nature of the phase transition that ended inflation at $\approx 10^{-35}$ seconds after the big bang). The low frequency parts of the spectrum reflect fairly recent history of the universe. For example, for inflationary cosmology, the “kink” in the spectrum at 10^{-16} Hz reflects the change in the expansion law from radiation- to matter-domination at $Z_{\text{eq}} \approx 6000$. Grishchuk has shown that in general, this type of mechanism (parametric amplification of zero-point fluctuations) produces a spectrum of the sort we have illustrated. However if the universe does not expand exponentially (constant $H(t)$), but “speeds up” and “slows down” (i.e. $H(t)$ increases and decreases) then this is reflected in the spectrum of Ω_{gw} which is no longer flat, but instead has characteristic increases and decreases, reflecting the changing values of $H(t)$ during the evolution of the universe.

5.2. Cosmic String Cosmology

In this lecture, I am going to show you a calculation of the stochastic gravitational wave background produced by a network of cosmic strings [34, 35]. These are objects which might have formed during a phase transition, as the universe cooled. We do not know if our universe contains cosmic strings or not (this depends upon the precise nature of the phase transition) so these calculations must be viewed as illustrative rather than realistic.

Cosmic strings are one-dimensional (in space) string-like objects. They are topologically-stable scalar/gauge field configurations, whose dominant decay mechanism is the emission of gravitational waves. These string-like objects are analogous to the vortex lines which form in superfluid helium, or to topological defects which can form during phase transitions of liquid crystals. Here, our interest is in cosmic strings which might have formed during a phase transition as the universe cooled, and a fundamental $U(1)$ local gauge symmetry was broken. These are the simplest strings; they are characterized by a single dimensional scale: their mass-per-unit-length μ . A phase transition which formed strings at the Grand Unified Theory (GUT) energy scale of about 10^{16} GeV would result in strings with $\mu \approx 10^{22}$ gms/cm.

These kinds of cosmic string have several remarkable properties. First, they are formed without any “ends” so the strings are always in the form of loops. Sometimes the loops are small (compared to the Hubble length) in which case we call them “loops”. Sometimes the loops are large (compared to the Hubble length) in which case we call them “infinite strings”. In neither case are there any unjoined “ends”. Note that in assigning a “length” to the loop, we are using an invariant measure of the length; the length is defined as the total energy of the loop divided by its mass-per-unit-length μ . A second remarkably property of these loops is that they have a tension equal to their mass-per-unit-length μ .

This is in contrast to the kind of strings we use to wrap packages, which have small tension compared to their mass-per-unit-length μ . Because of this large tension, the cosmic strings oscillate relativistically under their own tension. Thus, a circular loop of cosmic string, initially placed at rest, will collapse under its own tension in a time comparable to the time it takes a light ray to move a distance equal to the radius of the loop. In general, a non-circular loop will oscillate quasi-periodically, with a period equal to (half) the time it takes light to travel a distance equal to the length of the string making up the loop. A third remarkable property of these cosmic string loops is that they are stable against all types of decay apart from the emission of gravitational radiation. So typically a loop of cosmic string, under the effects of its own tension, will oscillate almost periodically, gradually emitting gravitational radiation, and shrinking in size.

One might worry that the configuration of these cosmic strings is very complicated, depending precisely upon how the mass-energy of the universe was distributed when they were formed, and that for this reason, it would be terribly difficult to make any precise predictions about the effects they would have on the universe. Fortunately, about fifteen years of extensive study of networks of cosmic string has revealed that they have a remarkable “scaling” property [34, 35]. This can be summarized by Fig. 13, which shows a snapshot (at one instant of cosmic time) of a universe containing cosmic strings. The crucial point is this one: at any instant in time, the appearance of the string network is (statistically) like that shown in the figure Fig. 13. As the universe expands, the string network evolves; however at any time, each Hubble sized volume contains, on the average, a certain number (say $A=52$) of infinite strings passing through it, and a very large number of small loops. The small loops oscillate, emitting gravitational radiation, and as the universe evolves, more small loops are chopped off the infinite strings, replacing those loops which are disappearing after converting their energy into gravitational waves. All of the properties of the network “scale” with the Hubble length. So even though it is *impossible* to predict the appearance of a string network in our own universe, in a statistical sense, we *can* describe the average properties of the network at any time.

The spectrum of gravitational radiation produced by a cosmic string network has been carefully studied [34, 35, 41, 42]. The spectrum of gravitational radiation produced by a “typical” cosmic string network is shown in Fig. 14. You can see that although the spectrum is not flat, it is fairly flat in the range of frequencies which LIGO and the other ground-based detectors will be sensitive to. This radiation was produced by loops which emitted during the epoch when the universe was still radiation-dominated. I want to show you an estimate of the amplitude of the stochastic spectrum $\Omega_{\text{gw}}(f)$ for the range of frequencies f over which Ω_{gw} is roughly constant. To do this, I need to carry out counting arguments, to count the number of loops emitting gravitational radiation at any time. The number of loops that we have depends upon the volume that we consider, and the counting gets tricky if we don’t make the right choice.

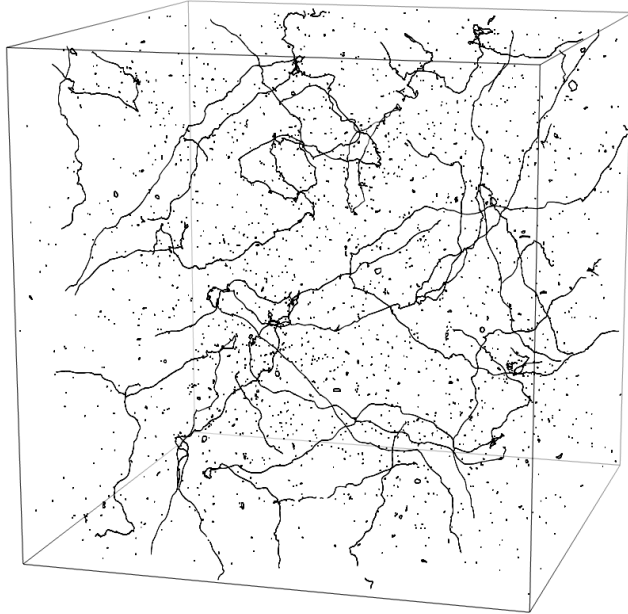


Fig. 13. — A snapshot of a universe containing a cosmic string network. The spatial volume shown here is a cube with side length $2c/H$ where H is the Hubble expansion rate. The string network has a remarkable scaling property: at any time the appearance of the network is (statistically) like the one shown here, provided that all length scales are expressed in terms of the Hubble length at that time. The network consists of many tiny loops, which here appear as points, and a number of so-called “infinite” strings. Although these infinite strings appear to have ends, this is just an artifact of having “cut out” a Hubble volume cube for this snapshot.

For example, we could choose a volume which at any time was a single Hubble volume (a ball of radius equal to the Hubble length), or we could pick a constant co-moving volume, or a fixed physical volume. To avoid the need to make one of these choices, there is a simpler way to do the counting. We’ll do our calculations for a universe which has a finite spatial volume, and whenever we count something (say loops), we’ll simply count the total number of those things (i.e. loops) in the *entire* universe.

The universe we will use is shown in Fig. 15. At any instant in time, its spatial topology is that of a three-dimensional torus $T^3 = S^1 \times S^1 \times S^1$. The metric is $ds^2 = -dt^2 + a^2(t)d\vec{x}^2$, but the spatial coordinates are each periodically identified on the interval $[0, L]$. Thus each of the three spatial coordinates

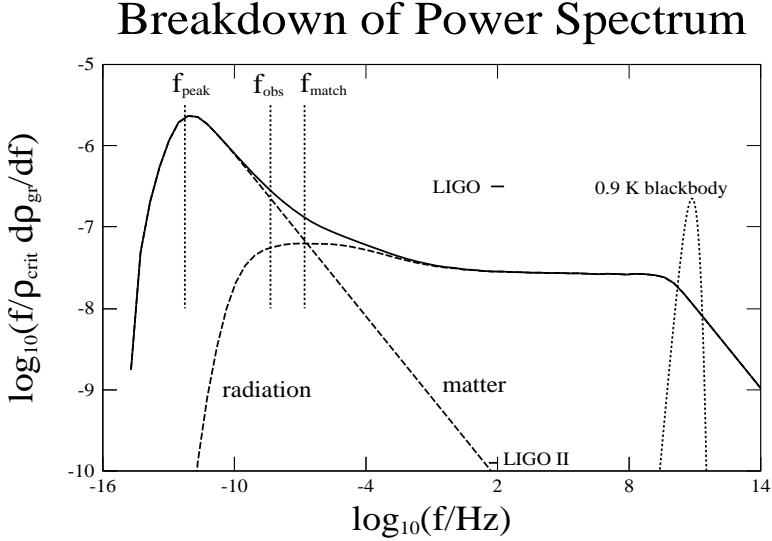


Fig. 14. — A typical spectrum of gravitational radiation produced by a cosmic string network is shown as the solid curve. The dotted curves show the contributions of loops which “died” while the universe was radiation-dominated, and the contributions of loops which “died” more recently, when the universe was matter-dominated. The part of the spectrum which lies in the LIGO band comes from the radiation-dominated epoch. Also shown, for naive comparison, is the spectrum of a 0.9 Kelvin blackbody. The frequency f_{obs} is where the millisecond pulsar timing observations constrain the spectrum.

ranges over $0 < x, y, z < L$. The time coordinate t is physical or comoving time, and during the radiation-dominated epoch of cosmological expansion, $a(t) = (t/t_0)^{1/2}$ where t_0 is the present time, related to the present Hubble expansion rate by $t_0 = (2H_0)^{-1}$. Our model universe has a finite proper spatial volume; at any instant in time this three volume is $V(t) = L^3 a^3(t)$. Provided that this volume is greater than the Hubble volume (in other words, t is less than some critical value) then the fact that our model universe is finite in spatial extent, rather than infinite, does not matter and observable quantities will have the same values that they would have in a truly infinite universe. So the toroidal topology of our model universe simply serves as a convenient calculational tool.

Shown in Fig. 16 is the spectrum of gravitational radiation produced by a cosmic string network described by a particular set of dimensionless parameters. This spectrum was actually calculated by a computer program [41, 42] ; there

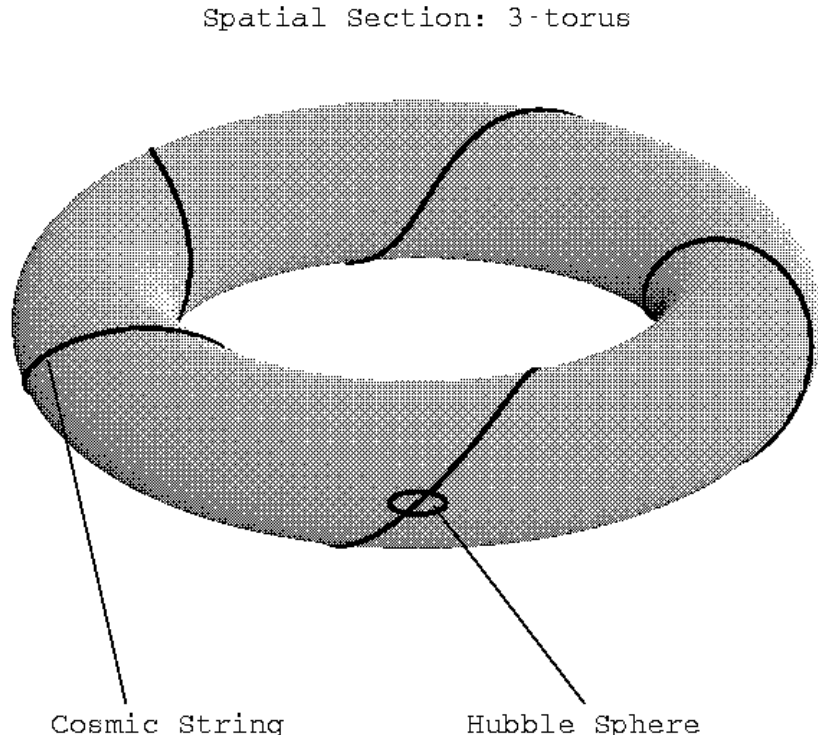


Fig. 15. — A spatial slice of the model universe, at one instant in time, is a three-dimensional torus. In the figure, we have shown a single long cosmic string, which winds around this universe 5 times in the x -direction and 1 time in the y -direction. Because the figure shows a two-dimensional projection, we can't see how many times the string winds around in the z -direction. Note that the string has no ends. Also shown is a small sphere, which is the boundary of the Hubble volume at the given instant in time. At later times, this small sphere would be larger, and would include a larger part of the three-torus. The single long string shown in this figure is a so-called “infinite” string. Although its length is finite and it has no ends, it is not called a “loop” because it is longer than the Hubble length.

is no way to write a useful analytic expression for this spectra. You will notice however that the LIGO frequency band (around 100 Hz) Ω_{gw} is flat (a constant, independent of frequency). It is not difficult to derive a formula for this constant value.

To analytically determine the amplitude of Ω_{gw} in the LIGO band, we will make extensive use of the scaling property of the string network. This property has been well established, both by computer simulation and by analytic

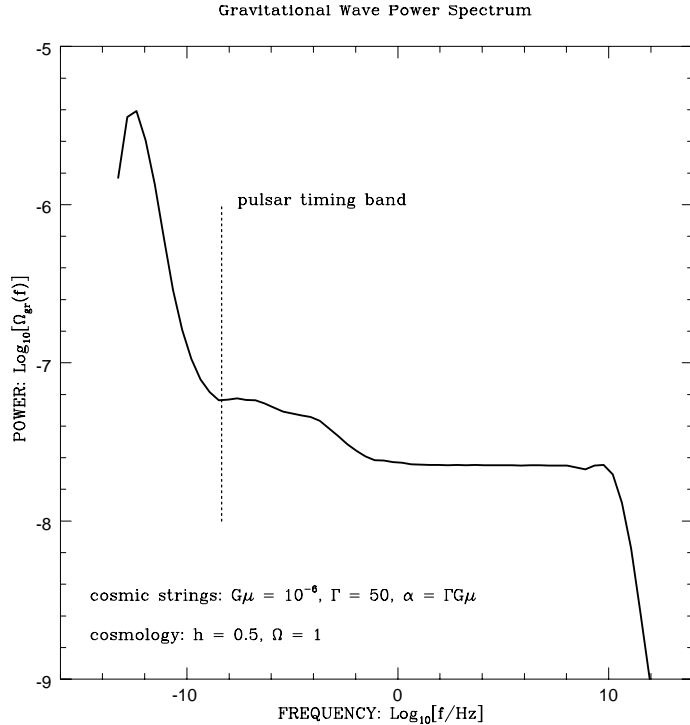


Fig. 16. — The spectrum of gravitational radiation produced by a cosmic string network. Around the LIGO frequency band $f \approx 100$ Hz, the spectrum is fairly flat. In these lectures, we derive a simple analytic estimate for the amplitude of Ω_{gw} in this flat region.

arguments [34, 35]. The scaling property may be neatly summarized: *A single correlation length $l(t) = \text{Hubble length} = 2t$ characterizes ALL properties of the string network.* This scaling property can be used to obtain qualitative relations. For example, the energy-density of long strings is given by

$$\rho_\infty = \frac{A\mu lc^2}{l^3} = \frac{A\mu}{4t^2}, \quad (78)$$

where μ is the mass-per-unit-length of the string, and A is a dimensionless constant (determined by numerical simulations to have a value $A \approx 52$). Roughly speaking, A is the number of long strings which pass through the Hubble volume shown in Fig. 13. (An example of such a long string passing through a Hubble volume is shown in Fig. 15.) Another example of scaling concerns the sizes of loops of string which are “chopped off” the infinite string network.

From scaling, the size of these loops at the time of formation must be

$$\text{Size of loop formed at } t_{\text{birth}} = \alpha c t_{\text{birth}}, \quad (79)$$

where α is a dimensionless constant (which in principle can be determined by numerical simulation).

Because the gravitational radiation produced by a cosmic string network comes from the small oscillating loops of string, we need to determine the rate at which these loops are formed. This can be found from energy conservation. The decrease in the total energy of long string in the universe must be compensated by a corresponding increase in the total energy of cosmic string loops:

$$d(V\rho_\infty) + (\mu a t c^3) dN_{\text{loops}} = 0. \quad (80)$$

(Note that the equation of state of the string loops is similar to that of dust; otherwise the equation of energy conservation would be somewhat more complicated.) Using the expressions above for ρ_∞ and for V we obtain an equation for the rate at which loops of string are formed:

$$\frac{dN_{\text{loops}}}{dt} = \frac{1}{8} \frac{L^3 A}{\alpha c^3} t_0^{-3/2} t^{-5/2}, \quad (81)$$

where I've used the explicit time dependence of $a(t)$. The loops which are being cut off the infinite strings oscillate relativistically, emitting gravitational radiation. A remarkable fact about these loops is that the energy-loss rate (power radiated) P does not depend upon the size of the loops, but only on their shape [34, 35]. For an “average” loop

$$P = \gamma G \mu^2 c, \quad (82)$$

where γ is a dimensionless constant, which has been determined numerically to have a value $\gamma \approx 50$. Because the loops radiate power at a constant rate, independent of their size, the energy and mass of a loop decrease linearly with time, until all the energy has been radiated away. At time t , a loop formed at time t_{birth} has length

$$(\text{Size of loop formed at } t_{\text{birth}}, \text{ at time } t) = \alpha c t_{\text{birth}} - \gamma G \mu (t - t_{\text{birth}})/c. \quad (83)$$

The loop disappears when this length reaches zero, at a time

$$t_{\text{death}} = \left(1 + \frac{\alpha c^2}{\gamma G \mu}\right) t_{\text{birth}} \equiv \beta t_{\text{birth}}, \quad (84)$$

where we have defined a constant $\beta = 1 + \frac{\alpha c^2}{\gamma G \mu} > 1$ which is the (constant) ratio of death-time to birth-time for cosmic string loops. We are now in a position to work out an analytic approximation to $\Omega_{\text{gw}}(f)$ for cosmic string networks, which is valid in the LIGO band.

Consider the total energy (as seen today) emitted in gravitational waves by all oscillating cosmic string loops which were formed (1) after the cosmic string network came into existence at time $t_{\text{formation}}$ and (2) which are no longer present, and thus were born before time t_0/β . This total energy is

$$E_{\text{gw}} = \int_{t_{\text{formation}}}^{t_0/\beta} dt' \frac{dN_{\text{loop}}}{dt'} \int_{t'}^{\beta t'} dt'' \gamma G \mu^2 c \frac{a(t'')}{a(t_0)} \quad (85)$$

$$+ (\text{Ignore Loops Still Present Today}). \quad (86)$$

The different factors appearing in this formula are (1) the number of loops dN_{loop} born in the time interval dt' , (2) the energy $dE = dt'' \gamma G \mu^2 c$ emitted by those loops in the time interval dt'' , and (3) the redshift factor $a(t'')/a(t_0)$ which reduces the energy as observed today. Substituting in expression (81) for the rate of loop formation and carrying out the integral over t'' gives

$$E_{\text{gw}} = \int_{t_{\text{formation}}}^{t_0/\beta} dt' \frac{dN_{\text{loop}}}{dt'} \left[\frac{2}{3} \gamma G \mu^2 c t_0^{-1/2} t'^{3/2} (\beta^{3/2} - 1) \right] \quad (87)$$

$$= \frac{1}{8} \frac{L^3 A}{\alpha c^2} t_0^{-2} \frac{2}{3} \gamma G \mu^2 (\beta^{3/2} - 1) \left[\ln \left(\frac{t_0}{t_{\text{formation}}} \right) - \ln \beta \right]. \quad (88)$$

Because of the scaling nature of the string network, the logarithmic frequency interval over which the gravitational radiation is distributed is precisely

$$\ln \left(\frac{f_{\text{high}}}{f_{\text{low}}} \right) = \ln \left(\frac{t_0}{t_{\text{formation}}} \right). \quad (89)$$

The $\ln \beta$ term can be neglected in comparison with the other \ln term, because typically the magnitude of $100 < \beta < 10^5$ is much smaller than the magnitude of $t_0/t_{\text{formation}} \approx 10^{50}$ for GUT scale strings. If we now use the relationship between the Hubble expansion rate and the critical energy density,

$$H_0^2 = \frac{1}{4t_0^2} = \frac{8\pi G \rho_{\text{critical}}}{3c^2} \quad (90)$$

we can immediately calculate the spectrum of gravitational waves:

$$\Omega_{\text{gw}} = \frac{1}{\rho_{\text{critical}}} \frac{d\rho_{\text{gw}}}{d \ln f} \quad (91)$$

$$= \frac{1}{\rho_{\text{critical}}} \frac{E_{\text{gw}}}{\ln(f_{\text{high}}/f_{\text{low}})} \frac{1}{L^3} \quad (92)$$

$$= \frac{1}{8} \frac{A}{\alpha c^2} \frac{32\pi G}{3c^2} \frac{2}{3} \gamma G \mu^2 (\beta^{3/2} - 1). \quad (93)$$

Now this calculation is for a radiation-dominated universe. If we include the phase of matter domination following it, the amplitude of the spectrum is decreased by a factor of $(1 + Z_{\text{eq}})$ to give our final result for the amplitude

of the stochastic gravity wave background of a cosmic string network, in the LIGO band:

$$\Omega_{\text{gw}} = \frac{8\pi}{9} \frac{A\gamma}{\alpha} \left(\frac{G\mu}{c^2} \right)^2 \left(\beta^{3/2} - 1 \right) (1 + Z_{\text{eq}})^{-1}. \quad (94)$$

This quantity can be large enough to be observable with the LIGO detectors, for values of the dimensionless parameters characterizing the cosmic strings.

The values of these dimensionless parameters are not completely known. Reasonable values are $A = 52$ for the number of long strings/horizon volume, $\gamma \approx 50$ (for the radiation rate from a typical loop) and mass-per-unit-length $G\mu/c^2 \approx 10^{-6}$ for GUT phase transitions. However the value of α (the size of a loop at formation) is still unknown. The high-resolution numerical simulations have established that $\alpha < 10^{-2}$ but this is only an upper bound. Indeed it is thought that α could perhaps be as small as $\gamma G\mu/c^2 \approx 10^{-5}$, which is the scale at which gravitational back reaction cuts off the small scale structure and fluctuations on the long strings [34, 35]. This uncertainty in the value of α leads to a wide uncertainty in β ; the allowed range is $\beta \in [1, 200]$. Because this parameter governs the lifetime of a loop, it has a large effect on the spectrum Ω_{gw} .

There is increasing evidence that the scale of loop formation (i.e. the value of α) is indeed set by gravitational back reaction, and is thus very small. One can work out the limit $\alpha \rightarrow 0$ of Ω_{gw} , obtaining

$$\Omega_{\text{gw}} = \frac{4\pi}{3} A \left(\frac{G\mu}{c^2} \right) (1 + Z_{\text{eq}})^{-1}. \quad (95)$$

This may well turn out to be the correct expression in the LIGO frequency range. However the allowable range of μ is tightly constrained by the millisecond pulsar timing observations discussed in Section 4.2, and the increasingly strong constraints of these observations may rule out GUT scale cosmic strings in the near future [41, 42].

5.3. Bubbles from First-Order Phase Transitions

My final example of a specific mechanism that can produce a stochastic background of gravitational radiation is rather different than the two previous examples I have examined (inflationary cosmology and cosmic strings). In these two previous examples there was a scaling law or behavior which resulted in a spectrum $\Omega_{\text{gw}}(f)$ that was flat, at least for waves which entered the Hubble sphere before the universe became matter-dominated.

In this final example, I will briefly review the effects of a different type of mechanism. In this mechanism, as the universe expands and cools, the matter within it undergoes a first-order phase transition at some definite time in the past [36, 37, 38]. This transition occurs when the temperature T_* of the universe has dropped sufficiently below the characteristic energy of the phase transition:

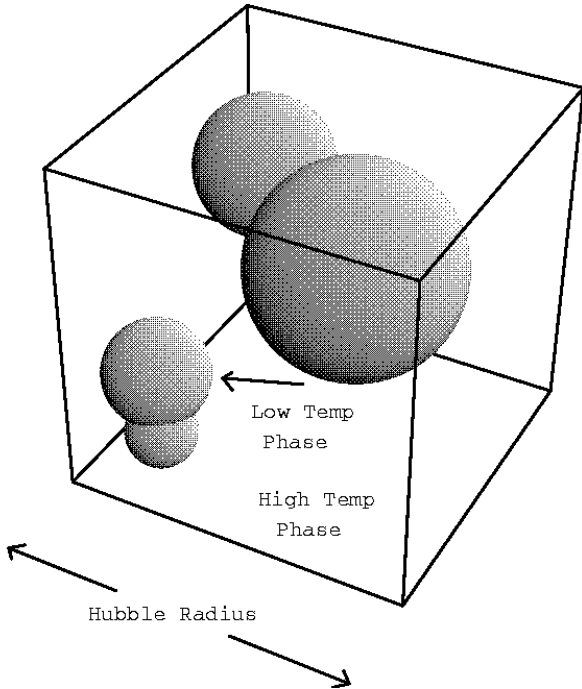


Fig. 17. — A first-order phase transition can produce rapidly-expanding bubbles containing the new (low temperature) phase within the old (high-temperature) phase. The difference in energy (latent heat) is transformed into kinetic energy of the bubble walls. When the bubbles collide, a fraction of this energy is emitted as gravitational radiation.

$kT_* < E_{\text{transition}}$. Bubbles of the new (low-energy-density) phase form within the old (high-energy-density) phase, as shown in Fig. 17. These bubbles expand rapidly after formation, converting the difference in energy density \times bubble volume into kinetic energy of the bubble walls. Within a short time, these bubbles are moving relativistically, and within a Hubble expansion time, they collide. These collisions are highly relativistic, non-symmetric events, and produce copious amounts of gravitational radiation. Within a short time after the collisions begin, a significant fraction of the energy that was in the bubble walls is converted into gravitational radiation.

In contrast to our previous two examples, this bubble collision process produces a spectrum which is strongly peaked at a particular frequency, charac-

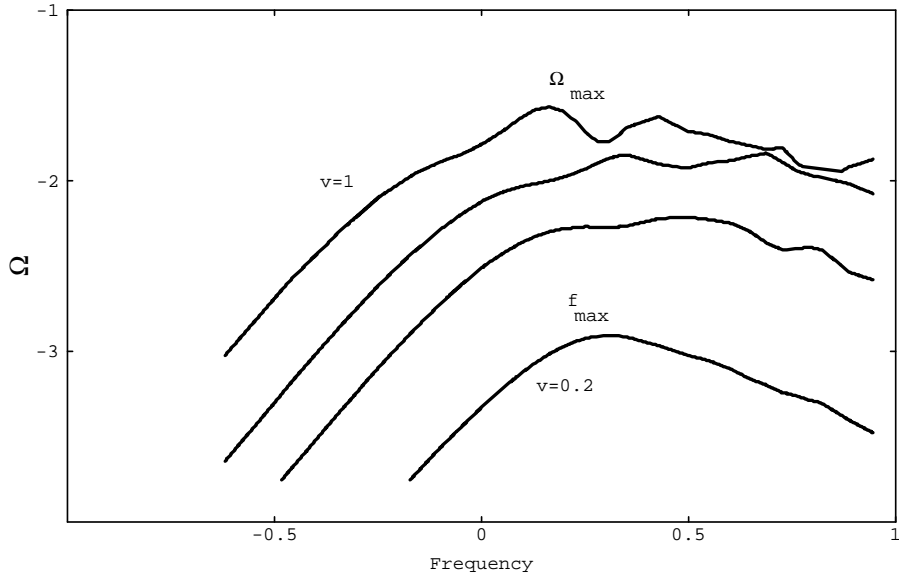


Fig. 18. — Typical spectra $\Omega_{\text{gw}}(f)$ produced from the collision of bubbles which result from a first-order phase transition. This graph is reproduced from Fig. 7 of Kamionkowski, Kosowsky, and Turner [36]. The horizontal axis is $\log_{10}(2\pi f/\beta)$ and the vertical axis is $\log_{10} \Omega_{\text{gw}} \beta^2 (1 + \alpha)^2 H^{-2} \alpha^{-2} \kappa^{-2}$. The spectrum peaks at a characteristic frequency f_{max} , characteristic of the expansion rate and time at which the bubble collisions occurred. The spectra are shown for bubble wall velocities of $v = 0.2, 0.4, 0.6$ and 1.0 .

teristic of the time at which the phase transition and bubble collisions took place. This spectrum has been computed [36, 37, 38] and is shown in Fig. 18. The spectrum is peaked at a characteristic frequency

$$f_{\text{max}} \approx 5.2 \times 10^{-8} \left(\frac{\beta}{H_*} \right) \left(\frac{T_*}{1 \text{ GeV}} \right) \left(\frac{g_*}{100} \right)^{1/6} \text{ Hz.} \quad (96)$$

The Hubble expansion rate at the time of the phase transition is denoted H_* and β is a measure of the bubble nucleation rate. For typical phase transitions, Kosowsky, Turner and their collaborators [36, 37, 38] find that $\beta/H_* \approx 4 \ln(M_{\text{Planck}}/T_*) \approx 10^2$. The number of degrees of freedom g_* is also of order 10^2 in typical GUT models. For example, in the minimal standard model electro-weak phase transition one has the transition at an energy $T_* \approx 10^2$ GeV with $f_{\text{max}} \approx 4.1 \times 10^{-3}$ Hz.

The amplitude of the spectrum depends mostly upon the relative energy-density difference between the interior and the exterior of a bubble. This dif-

ference in energy density is deposited directly in the bubble walls, determining the speed at which the walls crash together, and thus the amount of energy converted to gravitational radiation. The difference is described by a parameter $\alpha = \frac{\rho_{\text{vac}}}{\rho_{\text{thermal}}}$. Kosowsky, Turner and Watkins find that the amplitude of the spectrum at the peak is approximately

$$\Omega_{\text{gw}}(f_{\text{max}})h_{100}^2 \approx 1.1 \times 10^{-6} \kappa^2 \left(\frac{\beta}{H_*} \right)^{-2} \left(\frac{\alpha}{1+\alpha} \right)^2 \left(\frac{v^3}{0.24+v^3} \right) \left(\frac{g_*}{100} \right)^{-1/3}. \quad (97)$$

The parameter κ is the fraction of vacuum energy that goes into kinetic energy of the fluid; it is an increasing function of α and typically lies in the range $10^{-2} < \kappa < 1$. The final parameter v is the propagation velocity of the bubble walls. For strongly first-order phase transitions, $\alpha \rightarrow \infty$ and $v \rightarrow 1$. In this strongly first-order case, a phase transition at $\approx 10^9$ GeV could be easily observed with the Advanced LIGO detectors.

We should note that it is perhaps overly optimistic to assume that the phase transition is strongly first-order. At least one phase transition which is expected to occur, at an energy scale of about 10² GeV, is the electro-weak transition. In the standard SU(3) model this phase transition has $\Omega_{\text{gw}}(4.1 \times 10^{-3} \text{Hz}) \approx 10^{-22}$, which is many orders of magnitude too small to be observable by any proposed space-based detector [36, 37, 38]. However it is perfectly possible that there was a strongly first-order phase transition in the earlier history of the universe, that might give rise to wave observable with the proposed LISA detector.

6. Conclusion

I am often asked, after a series of lectures like this, “Do you really think that a stochastic background is there?” There is only one possible honest answer – I do not know! The problem is that we have very little information about what really happened in the very early universe. And the scenarios that we have given as examples are just that, examples. Personally, I think it is unlikely that any of them will turn out to be true. However they do have *illustrative* value. They show that, under reasonable assumptions about what happened in the early universe, it *is* possible to produce a stochastic background which is easily detected with the instruments now under construction.

So while the answer to the question is unknown, that does not matter. In the next decade we will probably know the answer in a very direct way, with real observational data. And if we do detect a stochastic background, a new era in our understanding of the early universe will begin.

Acknowledgments

This work has been partially supported by NSF grant PHY95-07740. I also thank Kip Thorne for his hospitality at Caltech, where much of this work was

completed, and for the support of his NSF grant PHY94-24337. I acknowledge B.S. Sathyaprakash for showing me the elegant argument which I have adapted at the end of Section 3.3, and useful conversations with Eanna Flanagan, Kip Thorne, Rai Weiss, Kent Blackburn, David Shoemaker, Ron Drever, Stan Whitcomb, and Robbie Vogt. I am also very grateful to Joseph Romano for his careful reading of this manuscript and many useful comments.

Appendix A

Calculational Details

The purpose of this section is to provide details of the calculations of the expectation values of the strains due to a stochastic background. The starting point is the plane wave expansion of the gravitational metric perturbations. In transverse traceless gauge, this can be written in the form of a plane wave expansion

$$h_{ab}(t, \vec{x}) = \sum_A \int d^3k C_A(\vec{k}) \sin(c|\vec{k}|t - \vec{k} \cdot \vec{x} + \Phi(\vec{k})) e_{ab}^A(\hat{k}). \quad (\text{A1})$$

Here $A = +, \times$ label the two polarization states, \vec{k} is the wave-vector of the perturbation, C_A are arbitrary real functions specifying the amplitude of the modes, Φ is a real function taking values in the interval $[0, \pi]$ and e_{ab}^A are the polarization tensors, which depend only upon the direction of the wave-vector \vec{k} . This decomposition is unique: every gravity wave can be represented exactly one way, in this form.

Rather than representing the traveling wave by a phase and a real amplitude, it is more convenient to use a complex amplitude. An equivalent representation is

$$h_{ab}(t, \vec{x}) = \Re \left(\sum_A \int_0^\infty df \int_{S^2} d\hat{\Omega} B_A(f, \hat{\Omega}) \exp(2\pi i f(t - \hat{\Omega} \cdot \vec{x}/c)) e_{ab}^A(\hat{\Omega}) \right) \quad (\text{A2})$$

Here, $\hat{\Omega}$ is a unit vector on the two-sphere; we have effectively written $\vec{k} = 2\pi f \hat{\Omega}$. The function $B_A(f, \hat{\Omega})$ is an arbitrary complex function of the two variables, defined on the range $f \geq 0$. By taking the real part of this expression explicitly, one can cast it in the form

$$h_{ab}(t, \vec{x}) = \sum_A \int_{-\infty}^\infty df \int_{S^2} d\hat{\Omega} h_A(f, \hat{\Omega}) \exp(2\pi i f(t - \hat{\Omega} \cdot \vec{x}/c)) e_{ab}^A(\hat{\Omega}), \quad (\text{A3})$$

where now $h_A(f, \hat{\Omega})$ is an arbitrary complex function satisfying the relation $h_A(-f, \hat{\Omega}) = h_A^*(f, \hat{\Omega})$. As before, this decomposition is unique.

The polarization tensors appearing in these relations may be given explicitly. In standard angular coordinates (θ, ϕ) on the sphere one has

$$\hat{\Omega} = \cos \phi \sin \theta \hat{x} + \sin \phi \sin \theta \hat{y} + \cos \theta \hat{z} \quad (\text{A4})$$

$$\hat{m} = \sin \phi \hat{x} - \cos \phi \hat{y} \quad (\text{A5})$$

$$\hat{n} = \cos \phi \cos \theta \hat{x} + \sin \phi \cos \theta \hat{y} - \sin \theta \hat{z} \quad (\text{A6})$$

$$e_{ab}^+(\hat{\Omega}) = m_a m_b - n_a n_b \quad (\text{A7})$$

$$e_{ab}^\times(\hat{\Omega}) = m_a n_b + n_a m_b \quad (\text{A8})$$

One can verify by inspection that \hat{m} and \hat{n} are a pair of orthogonal unit-length vectors in the plane perpendicular to $\hat{\Omega}$. It is simple to show that any rotation of the vectors \hat{m} and \hat{n} within the plane that they define simply corresponds to a trivial re-definition of the complex wave amplitudes h_+ and h_\times .

We are now in a position to verify some of our key formula. We begin with the assumption that the stochastic background is stationary and Gaussian. This means that the ensemble average of the Fourier amplitudes is

$$\langle h_A^*(f, \hat{\Omega}) h_{A'}(f', \hat{\Omega}') \rangle = \delta(f - f') \delta^2(\hat{\Omega}, \hat{\Omega}') \delta_{AA'} H(f) \quad (\text{A9})$$

for all f and f' . In these formula,

$$\delta^2(\hat{\Omega}, \hat{\Omega}') = \delta(\phi - \phi') \delta(\cos \theta - \cos \theta') \quad (\text{A10})$$

is the covariant Dirac δ -function on the two-sphere, and the covariant volume element is $d\hat{\Omega} = \sin \theta d\theta d\phi$. The function $H(f)$ is a real function related to the spectrum $\Omega_{\text{gw}}(f)$. $H(f)$ is a real, non-negative function, satisfying $H(f) = H(-f)$.

To see the relationship, consider the energy density in gravitational waves. This is given (locally) by

$$\rho_{\text{gw}} = \frac{c^2}{32\pi G} \langle \dot{h}_{ab} \dot{h}^{ab} \rangle, \quad (\text{A11})$$

where the overdot denotes a time derivative, and both tensors are evaluated at the same space-time point (t, \vec{x}) . Substituting the plane wave expansion into this formula yields

$$\langle \dot{h}_{ab}(t, \vec{x}) \dot{h}^{ab}(t, \vec{x}) \rangle = \sum_A \int_{-\infty}^{\infty} df \int_{S^2} d\hat{\Omega} 4\pi^2 f^2 H(f) e_{ab}^A(\hat{\Omega}) e_A^{ab}(\hat{\Omega}). \quad (\text{A12})$$

Since $\sum_A e_{ab}^A e_A^{ab} = 4$ and $\int d\hat{\Omega} = 4\pi$ one has

$$\langle \dot{h}_{ab} \dot{h}^{ab} \rangle = 64\pi^3 \int_{-\infty}^{\infty} df f^2 H(f) = 128\pi^3 \int_0^{\infty} df f^2 H(f). \quad (\text{A13})$$

Using the definition Ω_{gw} one obtains the relationship between the spectrum Ω_{gw} and $H(f)$. For $f \geq 0$ one has

$$\Omega_{\text{gw}}(f) = \frac{f}{\rho_{\text{critical}}} \frac{d\rho_{\text{gw}}}{df} = f \frac{8\pi G}{3c^2 H_0^2} \frac{c^2}{32\pi G} 128\pi^3 f^2 H(f) = \frac{32\pi^3}{3H_0^2} f^3 H(f). \quad (\text{A14})$$

This formula is needed to obtain the next result.

The second relation required is the expected value of the Fourier amplitudes at two different sites. This is now easily obtained. By definition

$$\begin{aligned} & \langle \tilde{h}_1^*(f) \tilde{h}_2(f') \rangle \\ &= \sum_{AA'} \int_{S^2} d\hat{\Omega} \int_{S^2} d\hat{\Omega}' \langle h_A^*(f, \hat{\Omega}) h_{A'}(f', \hat{\Omega}') \rangle \\ & \quad \times \exp(2\pi i f \hat{\Omega} \cdot \vec{x}_1/c - 2\pi i f' \hat{\Omega}' \cdot \vec{x}_2/c) F_1^A(\hat{\Omega}) F_2^{A'}(\hat{\Omega}') \\ &= \sum_A \int_{S^2} d\hat{\Omega} H(f) \exp(2\pi i f \hat{\Omega} \cdot \Delta \vec{x}/c) F_1^A(\hat{\Omega}) F_2^A(\hat{\Omega}) \delta(f - f') \\ &= \frac{8\pi}{5} \gamma(f) H(f) \delta(f - f') = \frac{3H_0^2}{20\pi^2} |f|^{-3} \Omega_{\text{gw}}(|f|) \gamma(|f|) \delta(f - f'). \end{aligned}$$

In the third line above, we have used the definition of the strain in the detector, given in (20), and in the fourth line, we have used the definition of the overlap reduction function (19).

References

- [1] Abramovici, A., et. al., *Science* **256** (1992) 325.
- [2] Caron, B., et. al., in Gravitational Wave Experiments (proceedings of the Edoardo Amaldi Conference, World Scientific, 1995) p. 86.
- [3] Danzmann, K., et. al, in Gravitational Wave Experiments (proceedings of the Edoardo Amaldi Conference, World Scientific, 1995) p. 100.
- [4] Tsubono, K., et. al, in Gravitational Wave Experiments (proceedings of the Edoardo Amaldi Conference, World Scientific, 1995) p. 112.
- [5] Thorne, K. S., in Particle and Nuclear Astrophysics and Cosmology in the Next Millennium (eds. E. W. Kolb and R. Peccei, World Scientific, 1995) p. 160.
- [6] Schutz, B. F. , in The Detection of Gravitational Waves (ed. D. G. Blair, Cambridge University Press, 1991) p. 406.
- [7] Blanchet, L., Damour, T., Iyer, B. R., Will, C. M., Wiseman, A. G., *Phys. Rev. Lett.* **74** (1995) 3515.
- [8] Apostolatos, T. A., Cutler, C., Sussman, G. J., Thorne, K. S., *Phys. Rev. D* **49** (1994) 6274.
- [9] Tagoshi, H., Sasaki, M., *Prog. Theor. Phys.* **92** (1994) 745.
- [10] Dhurandhar, S. V., Sathyaprakash, B. S., *Phys. Rev. D* **49** (1994) 1707.

- [11] Apostolatos, T. A., *Phys. Rev. D* **52** (1995) 605.
- [12] Owen, B., Search templates for gravitational waves from inspiralling binaries: choice of template spacing, Caltech Preprint, QC-9511032, November 1995, submitted to Physical Review D.
- [13] Niebauer, T.M., et. al, *Phys. Rev. D* **47** (1993) 3106.
- [14] Michelson, *Mon. Not. Roy. Astron. Soc.* **227** (1987) 933.
- [15] Christensen, N. *Phys. Rev. D* **46** (1992) 5250.
- [16] Flanagan, E. *Phys. Rev. D* **48** (1993) 2389. Note that the second term on the r.h.s. of equation (b6) should read $-10j_1(\alpha)$ rather than $-2j_1(\alpha)$, and that the sliding delay function shown in Figure 2 on page 2394 is incorrect.
- [17] Kolb, E. W., Turner, M., *The Early Universe* (Frontiers in Physics, Addison Wesley, 1990) p. 1.
- [18] Thorne, K. S., in *300 Years of Gravitation* (eds. S. Hawking W. Israel, Cambridge University Press, Cambridge, 1987) p. 330.
- [19] Hawking, S. W., Ellis, G. F. R., *The Large Scale Structure of Spacetime* (Cambridge University Press, Cambridge, 1973) p. 141.
- [20] Weinberg, S., *Gravitation and Cosmology: Principles and Applications of the General Theory of Relativity* (John Wiley & Sons, New York, 1972) p. 513.
- [21] Hough, J., et. al., in *Gravitational Wave Experiments* (proceedings of the Edoardo Amaldi Conference, World Scientific, 1995) p. 50.
- [22] Smoot, G. F., et. al, *Astrophys. J.* **396** (1992) L1.
- [23] Bennett, C. L., et. al, *Astrophys. J.* **396** (1992) L7.
- [24] Wright, E. L., et. al, *Astrophys. J.* **396** (1992) L13.
- [25] Bennett, C. L., et. al, *Astrophys. J.* **436** (1994) 423.
- [26] Bennett, C. L., et. al, Four Year COBE DMR Cosmic Microwave Background Observations: Maps and Basic Results, astro-ph/9601067, submitted to *Astrophys. J. Lett.*
- [27] Sachs R. K., Wolfe A. M., *Astrophys. J.* **147** (1967) 73.
- [28] Allen, B., Koranda, S. *Phys. Rev. D* **50** (1994) 3713.
- [29] Koranda, S., Allen, B. *Phys. Rev. D* **52** (1995) 1902.
- [30] Kaspi, V., Taylor, J., Ryba, M., *Astrophys. J.* **428** (1994) 713.
- [31] Thorsett, S. E., Dewey, R. J., *Phys. Rev. D* **53** (1996) 3468.
- [32] McHugh, M.P., Zalamansky, G., Vernotte, F., Lantz, E., Preprint, Besancon Observatory, March 1996.
- [33] Linde, A. D., *Particle Physics and Inflationary Cosmology* (Harwood, Chur, Switzerland, 1990) p. 1.
- [34] Vilenkin, A. *Phys. Rep.* **121** (1985) 263.
- [35] Vilenkin, A., Shellard, S., *Cosmic Strings and other Topological Defects* (Cambridge University Press, Cambridge, 1994) p. 1.
- [36] Kamionkowski, M., Kosowsky, A., Turner, M. S., *Phys. Rev. D* **49** (1994) 2837.
- [37] Kosowsky, A., Turner, M. S., Watkins, R., *Phys. Rev. D* **45** (1992) 4514.
- [38] Kosowsky, A., Turner, M. S., *Phys. Rev. D* **47** (1993) 4372.

- [39] Allen, B., *Phys. Rev. D* **37** (1988) 2078.
- [40] Birrell, N. D., Davies, P. C. W., *Quantum fields in curved space* (Cambridge University Press, Cambridge, 1982) p. 1.
- [41] Caldwell, R. R., Allen, B., *Phys. Rev. D* **45** (1992) 3447.
- [42] Caldwell, R. R., in *Proceedings of the fifth Canadian General Relativity and Gravitation Conference* (eds. R. McLenaghan and R. Mann, World Scientific, 1993) p. 1.